HHS Public Access

Author manuscript

Mol Cell. Author manuscript; available in PMC 2018 June 08.

Published in final edited form as:

Mol Cell. 2017 November 16; 68(4): 731–744.e9. doi:10.1016/j.molcel.2017.11.004.

Harnessing BET Inhibitor Sensitivity Reveals AMIGO2 as a Melanoma Survival Gene

Barbara Fontanals-Cirera[1,6], **Dan Hasson**[2,6], **Chiara Vardabasso**[2], **Raffaella Di Micco**[1,7], **Praveen Agrawal**[1], **Asif Chowdhury**[2], **Madeleine Gantz**[2], **Ana de Pablos-Aragoneses**[1], **Ari Morgenstern**[1], **Pamela Wu**[3], **Dan Filipescu**[2], **David Valle-Garcia**[2], **Farbod Darvishian**[1], **Jae-Seok Roe**[4], **Michael A. Davies**[5], **Christopher R. Vakoc**[4], **Eva Hernando**[1,*], and **Emily Bernstein**[2,8,*]

[1]Department of Pathology and Interdisciplinary Melanoma Cooperative Group, New York University Langone Medical Center, New York, NY, USA

[2]Departments of Oncological Sciences and Dermatology, 1470 Madison Avenue, Icahn School of Medicine at Mount Sinai, New York, NY, USA

[3]Institute of Systems Genetics, New York University Langone Medical Center, New York, NY, USA

[4]Cold Spring Harbor Laboratory, 1 Bungtown Road, Cold Spring Harbor, NY, USA

[5]Department of Melanoma Medical Oncology, The University of Texas MD Anderson Cancer Center, Houston, TX, USA

SUMMARY

Bromodomain and extraterminal domain inhibitors (BETi) represent promising therapeutic agents for metastatic melanoma, yet their mechanism of action remains unclear. Here we interrogated the transcriptional effects of BETi and identified AMIGO2, a trans-membrane molecule, as a BET target gene essential for melanoma cell survival. AMIGO2 is upregulated in melanoma cells and tissues compared to human melanocytes and nevi, and AMIGO2 silencing in melanoma cells induces G1/S arrest followed by apoptosis. We identified the pseudokinase PTK7 as an AMIGO2 interactor whose function is regulated by AMIGO2. Epigenomic profiling and genome editing revealed that *AMIGO2* is regulated by a melanoma-specific BRD2/4-bound promoter and super-enhancer configuration. Upon BETi treatment, BETs are evicted from these regulatory elements, resulting in AMIGO2 silencing and changes in PTK7 proteolytic processing. Collectively, this

[*]Correspondence: eva.hernando-monge@nyumc.org (E.H.), emily.bernstein@mssm.edu (E.B.).
[6]These authors contributed equally
[7]Present address: San Raffaele Telethon Institute for Gene Therapy (SR-Tiget), Via Olgettina 58, Milan, Italy
[8]Lead Contact

AUTHOR CONTRIBUTIONS

Conceptualization, B.F.-C., R.D.M., D.H., E.H., C.V., and E.B.; Investigation, B.F.-C., D.H., C.V., P.A., A.C., M.G., A.D.P.-A., A.M., and D.F.; Formal analysis, D.H., D.V.-G. and P.W.; Writing – Original Draft, B.F.-C., D.H., E.H., and E.B.; Writing – Review & Editing, B.F.-C., D.H., C.V., R.D.M., E.H., and E.B.; Visualization, D.H.; Resources, J.-S.R., C.R.V., and M.A.D.; Data Curation, F.D.; Supervision, M.A.D., E.H., and E.B.; Funding Acquisition, D.H., E.H., and E.B.

SUPPLEMENTAL INFORMATION

Supplemental Information includes seven figures and seven tables and can be found with this article online at https://doi.org/10.1016/j.molcel.2017.11.004.

study uncovers mechanisms underlying the therapeutic effects of BETi in melanoma and reveals the AMIGO2-PTK7 axis as a targetable pathway for metastatic melanoma.

Graphical Abstract

In Brief BET proteins play a central role in melanoma maintenance. By interrogating the effects of BET inhibition on melanoma transcriptional programs and regulatory elements, Fontanals-Cirera and Hasson et al. identified the transmembrane protein AMIGO2 as a survival factor whose expression is regulated by BET- and FOSL/TEAD-bound DNA regulatory elements.

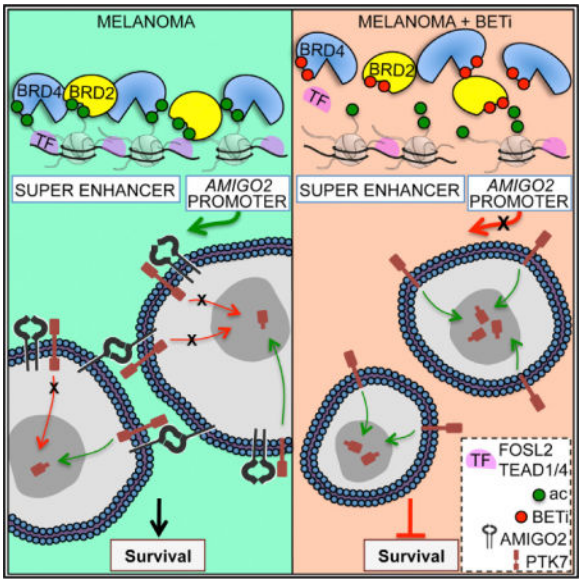

INTRODUCTION

Melanoma is the most aggressive form of skin cancer, with rising incidence (Whiteman et al., 2016). Melanoma development and progression have been mainly attributed to genetically altered oncogenes (e.g., *BRAF*, *NRAS*) and tumor suppressors (e.g., *CDKN2A*, *PTEN*, *NF1*) (Hodis et al., 2012), some of which have provided the basis for the development of effective targeted therapies (e.g., mutant-BRAF and MEK inhibitors) (Chapman et al., 2011; Kim et al., 2013). Agents targeting the immune microenvironment (e.g., anti-CTLA-4 and anti-PD-1/PD-L1) have also shown efficient and durable responses (Postow et al., 2015). Collectively, however, these therapies are administered to particular subsets of patients and relapse with treatment-refractory disease, and/or significant toxicities commonly occur (Fecher et al., 2013; Lito et al., 2013). While these approaches have significantly improved outcome for some metastatic melanoma patients, their limitations underscore the need for new therapeutic strategies.

Deregulation of the epigenome has emerged as a critical step in the activation and maintenance of aberrant transcriptional programs in melanoma pathogenesis (Ceol et al., 2011; Kapoor et al., 2010; Lian et al., 2012; Souroullas et al., 2016; Vardabasso et al., 2015; Zingg et al., 2015), which provides a basis for targeting chromatin regulators as a viable anti-cancer strategy. Particularly appealing are pharmacological compounds that displace

factors involved in transcriptional regulation from chromatin, such as the BET proteins (Dawson et al., 2011; Filippakopoulos and Knapp, 2014; Gallagher et al., 2014; Mertz et al., 2011; Puissant et al., 2013; Segura et al., 2013). The BET family consists of BRD2, BRD3, BRD4, and BRDT (testis-specific), which are “readers” of acetyl-lysine residues and recruit chromatin-modifying enzymes and transcriptional regulators to DNA regulatory elements. BRD4 is enriched at promoters, enhancers, and clusters of enhancers, termed super-enhancers (SEs), where it interacts with transcription factors (TFs) and components of the transcriptional machinery to promote expression of lineage-specific genes (Adam et al., 2015; Heinz et al., 2015; Whyte et al., 2013; Di Micco et al., 2014), while BRD2 binds to promoters occupied by the histone variant H2A.Z (Draker et al., 2012; Surface et al., 2016; Vardabasso et al., 2015) and a subset of CTCF binding sites, where it maintains transcriptional boundaries (Hsu et al., 2017).

Our groups and others reported that BRD2 and BRD4 are overexpressed in melanoma tissues and are essential for tumor maintenance (Gallagher et al., 2014; Segura et al., 2013; Vardabasso et al., 2015). Silencing of BRD2 and BRD4, as well as BET inhibition, impairs melanoma growth, suggesting that BETs regulate pro-proliferative and/or survival genes (Gallagher et al., 2014; Segura et al., 2013; Vardabasso et al., 2015). In turn, we hypothesized that examining the transcriptional programs of BET inhibition would (1) reveal novel melanoma-promoting genes that are not necessarily genetically altered, (2) expose molecular vulnerabilities that can be exploited therapeutically, and (3) provide a mechanistic understanding of BETi anti-tumoral effects that could further support their use for melanoma patients.

Here, we integrated the transcriptional signature of BET inhibition in melanoma with genes that are significantly upregulated relative to normal human melanocytes (NHM), in order to identify melanoma pro-tumorigenic factors. A loss-of-function screen of a subset of these genes and subsequent functional characterization uncovered *AMIGO2*, which encodes a type I transmembrane protein of the leucine-rich repeat (LRR) and Ig-like super family, as a melanoma survival gene. AMIGO2 is upregulated in melanoma tissues, and its silencing significantly impairs melanoma growth. Through a mass spectrometry study, we identified PTK7, a pseudo-tyrosine kinase, as an AMIGO2 interactor. We further demonstrated that AMIGO2 regulates PTK7 function and that PTK7 is also required for melanoma cell survival.

To address BET-mediated *AMIGO2* transcription, we characterized the melanoma enhancer landscape. We found *AMIGO2*, as well as additional pro-tumorigenic genes, to be associated with SEs not present in NHMs. Upon BET inhibition, BRD2 and BRD4 are displaced from a subset of melanoma SEs and corresponding promoters, resulting in decreased expression of SE-associated genes. We identified enrichment of FOSL2 and TEAD4 TFs at melanoma SEs, including those of *AMIGO2*, which directly regulate its expression. Together, our data indicate that *AMIGO2* is sensitive to BETi, displays increased expression in melanoma tissues, and acquires BET-regulated SEs in melanoma. Moreover, AMIGO2 is required for melanoma survival and interacts with pro-survival receptor PTK7. Our study further illustrates the value of leveraging the BETi-associated transcriptome as an effective strategy to identify pro-tumorigenic genes and therapeutic targets in melanoma.

RESULTS

Transcriptional Profiling of BETi-Treated Melanoma Cells Reveals Putative Pro-tumorigenic Genes

We utilized BETi to examine the BET-regulated transcriptome of malignant melanoma. These diazepine-based small molecules occupy the N-terminal tandem bromodomains of BETs and impair their binding to acetylated lysines (Filippakopoulos and Knapp, 2014). Two BETi-sensitive melanoma cells of distinct genetic background (SKmel147, $NRAS^{Q61R}$ and 501MEL, $BRAF^{V600E}$) were treated with JQ1 (JQ1[+]) and enantiomer (JQ1[−]) (Filippakopoulos et al., 2010) for 6 and 24 hr, followed by RNA sequencing (RNA-seq) (Figures 1A and S1A; Table S1). BETi led to significant transcriptional changes at 6 hr, which were sustained at 24 hr of treatment (Figures S1B and S1C). By further examining genes downregulated in both melanoma cell lines at 6 hr, at 24 hr, or at both time points, we identified a core network of ~800 JQ1-sensitive genes (Figures 1A and 1B; Table S1). Gene ontology (GO) classification showed enrichment for gene functions such as regulation of cell cycle (Figure S1D), consistent with the proliferative arrest observed following BET inhibition (Segura et al., 2013; Vardabasso et al., 2015).

Next, we determined the genes that are overexpressed in melanoma cells compared to NHMs (Figures 1A and S1E) and identified ~600 common to both melanoma cell lines (Figure 1C; Table S1). GO analysis showed that these genes are involved in cell-cycle and organelle assembly, among others (Figure S1F). Integration of the JQ1-sensitive gene signature with genes upregulated in melanoma relative to NHMs (Figure 1A) revealed 78 putative pro-tumorigenic genes (Figure 1D; Table S1). GO classification showed enrichment of gene functions including regulation of DNA metabolic processes, mitosis, and negative regulation of neurogenesis (Figure S1G), supporting their roles in melanoma.

Candidate Loss-of-Function Proliferation Screen Reveals *AMIGO2*

To assess the functional significance of these genes, we selected eight (of the 78 candidates) with little to no evidence of involvement in melanoma pathogenesis, and one positive control gene, *HMGA2* (Raskin et al., 2013; Zhang et al., 2015), to be tested in a loss-of-function mini-screen. We transiently transfected SKmel147 cells with siRNA pools against each of the nine genes and assessed their impact on proliferation (Figure 1E). Silencing of *HMGA2* showed the most significant proliferation defect. Four additional genes, *AMIGO2*, *MED25*, *ZIC1*, and *ZBTB38*, scored significantly (Figure 1E), functionally identifying them as regulators of melanoma cell growth. We validated that these genes are transcriptionally downregulated upon JQ1 treatment in 501MEL and SKmel147 cells by quantitative RT-PCR (qRT-PCR) (Figure S1H). Notably, *AMIGO2* (1) was significantly downregulated at both time points of JQ1 treatment (Figures 1D and S1H), (2) was also sensitive to a clinically relevant BETi, I-BET762 (Mirguet et al., 2013) (Figure 1F), and (3) represents a BETi-sensitive gene across multiple melanoma cell lines (Figure 1G). Based on these findings and the fact that AMIGO2 is a transmembrane molecule, which holds potential as a drug target, we investigated this gene for its role in melanoma biology.

AMIGO2 Is Upregulated in Human Melanoma

We assessed *AMIGO2* expression by qRT-PCR in a panel of melanoma cell lines and NHMs and found that *AMIGO2* is higher in most melanomas irrespective of genotype (Figure 2A). AMIGO2 is also upregulated at the mRNA and protein levels in patient-derived melanoma short-term cultures (STCs) (de Miera et al., 2012) (Figures 2B and 2C). Furthermore, expression data of two independent cohorts of human patient samples (TCGA Research Network and Xu et al., 2008) show significant upregulation in metastatic versus primary melanoma samples (Figure 2D) and show that *AMIGO2* expression is independent of mutational status (Figure 2E). We also found significantly increased AMIGO2 protein levels in primary and metastatic melanomas compared to skin melanocytes and nevi by immunohistochemistry using a tissue microarray (Figures 2F–2H; Table S2). All NHMs in skin were negative for AMIGO2; ~38% of nevi scored positively, while primary and metastatic melanomas scored 48% and 67%, respectively. In sum, AMIGO2 mRNA and protein levels are significantly higher in human melanoma relative to NHMs, independent of the driver mutation.

AMIGO2 Functions as a Pro-proliferation and Pro-survival Factor *In Vitro* and *In Vivo*

To assess the effects of AMIGO2 loss of function on melanoma survival, we stably suppressed its expression using four independent shRNAs (Figure S2A). *AMIGO2* silencing impaired melanoma cell proliferation and colony formation in 501MEL and SKmel147 cells (Figures 3A, 3B, S2B, and S2C) and in additional melanoma cell lines irrespective of genetic background (Figure S2D). To gain a mechanistic understanding of this phenotype, we investigated the effects of *AMIGO2* knockdown. Depletion of *AMIGO2* resulted in cell-cycle arrest via accumulation of cells in G1 and concomitant decrease in S phase cells (Figure 3C). This G1 arrest was followed by apoptosis marked by an increase in Annexin V-positive cells and Caspase-3 activity, which were both blocked by the addition of a pan-Caspase inhibitor, Q-VD-OPh (Kuželová et al., 2011), coupled to an increase in PARP cleavage (Figures 3D–3F and S2E–S2G). *AMIGO2* knockdown in NHMs did not alter their ability to proliferate (Figure S2H).

To investigate the consequences of *AMIGO2* silencing *in vivo*, SKmel147 cells stably expressing control (shSCR) or sh*AMIGO2* were injected into the flanks of immunocompromised mice. Cells expressing sh*AMIGO2* showed significant reduction in tumor growth and mass versus controls (Figures 3G and 3H), further supporting a role for AMIGO2 in proliferation and survival. Together, our data indicate that AMIGO2 is essential for melanoma growth both *in vitro* and *in vivo*.

Proteomic and Transcriptomic Analyses in the Context of AMIGO2 Deficiency

To molecularly characterize the role of AMIGO2 in melanoma, we conducted RNA-seq and reverse phase protein array (RPPA) (Park et al., 2010) of sh*AMIGO2*-versus shSCR-expressing 501MEL and SKmel147 cells. RPPAs are antibody arrays that include ~300 antibodies that detect either total protein or specific post-translational modifications of proteins, many of which are involved in signaling pathways. RNA-seq analysis identified ~1,500 deregulated genes upon *AMIGO2* depletion in both melanoma cell lines (Figure S3A; Table S1), five of which were also significantly altered by RPPA (Figures S3A and

S3B; Table S3). GO analysis of the RNA-seq revealed enrichment in pathways involved in cell division and proliferation (Figure S3C), consistent with the phenotypic effects of *AMIGO2* knockdown. Interestingly, RPPA analysis did not show significant and/or consistent changes in components of the MAPK signaling pathway (Figure S3D), but did reveal significant changes in FOXM1 (Figures S3B and S3E; Table S3), a TF implicated in melanoma proliferation by promoting cell-cycle progression (Bhat et al., 2008; Ito et al., 2016; Miyashita et al., 2015). Thus, our profiling data suggest that AMIGO2 loss results in transcriptional changes affecting proliferation prior to cell death.

The AMIGO2-PTK7 Axis Mediates Melanoma Survival

To link deficiency of AMIGO2, a transmembrane protein, with downstream transcriptional changes driving cell-cycle arrest and apoptosis, we investigated AMIGO2 protein interactors by affinity purification followed by mass spectrometry. We expressed an AMIGO2-GFP fusion protein, which properly localizes at the membrane in melanoma cells (Figure 4A), and found 159 unique interactors (Table S4). GO analysis showed enrichment in biological processes in which AMIGO2 has been implicated (e.g., cell adhesion, neuron projection) (Figure 4B) (Kuja-Panula et al., 2003). We validated AMIGO2 interaction with five transmembrane proteins (ALCAM, L1CAM, NRP1, NRP2 and PTK7) (Figures 4C, S4A, and S4B) with reported roles in cancer (Penna et al., 2013; Prud'homme and Glinka, 2012; Valiente et al., 2014). PTK7 was a consistent interactor across melanoma cell lines (Figures 4C and S4B) and co-localizes with AMIGO2 at the cell membrane (Figure S4C).

PTK7 is a kinase-dead receptor essential for neural tube formation and altered in cancer (Chen et al., 2014; Golubkov et al., 2014; Lu et al., 2004). We investigated whether PTK7 silencing would mimic the pro-apoptotic effects of AMIGO2 loss. PTK7 knockdown with two independent shRNAs (Figures 4D and S4D) significantly impaired cell growth and induced apoptosis in two melanoma cell lines (Figures 4E and 4F), with concomitant reduction of FOXM1 (Figures 4D and S4D). Thus, PTK7 knockdown phenocopies AMIGO2 silencing.

Like other membrane receptors, PTK7 function is regulated by proteolytic processing (Golubkov et al., 2011; Na et al., 2012). Upon proteolysis by MMP1 or ADAM17, a membrane-bound C-terminal fragment of PTK7 (CTF1) is generated. Further intra-membrane proteolysis by γ-secretase renders CTF2, which translocates to the nucleus (Figure S4E) and has been suggested to modulate gene expression (Na et al., 2012). We next queried whether AMIGO2 deficiency would alter the processing of PTK7. Indeed, we found that AMIGO2 knockdown results in accumulation of CTF1 and CTF2 (Figure 4G). These findings could be replicated by JQ1 treatment (Figure 4H). Upon AMIGO2 knockdown, we also found increased levels of nuclear CTF2 (Figure 4I). Collectively, our data suggest that AMIGO2 and PTK7 work together to promote melanoma cell survival and that AMIGO2 regulates PTK7 function.

Melanoma SEs Often Associate with Genes Encoding Pro-tumorigenic Factors

Next, we investigated the mechanisms underlying *AMIGO2* up-regulation in melanoma. Given that oncogene expression and BETi sensitivity are associated with BET occupancy at

SEs and promoters (Lovén et al., 2013), we hypothesized that *AMIGO2* expression could be driven by BET-occupied enhancers formed during melanocytic transformation. To map melanoma enhancers, we conducted chromatin immunoprecipitation coupled to high-throughput sequencing (ChIP-seq) for BRD4 as a marker of active enhancers (Lovén et al., 2013) and identified 464 SEs and 4,678 typical enhancers (TEs) in SKmel147 cells, also enriched for BRD2 (Figures 5A and 5B; Table S5). These enhancers were enriched for H3K27ac and MED1, as previously reported (Lovén et al., 2013; Whyte et al., 2013) (Figure S5A). We also identified enhancers based on H3K27ac (Lovén et al., 2013; Whyte et al., 2013), which yielded 1,040 SEs and 12,712 TEs, also enriched for BET proteins (Figures S5B–S5D; Table S5).

We next linked BRD4-identified SEs and TEs to their associated genes and identified 387 and 2,537 genes, respectively, which showed BRD4 and BRD2 enrichment at their promoters (Figures 5B, 5C, and S5E; Table S5). We found SE-associated genes to be expressed at higher levels and with higher expression levels over NHMs compared to non-TE-/non-SE- and TE-associated genes, and more sensitive to BETi (Figure 5D). Consistent with previous reports (Anders et al., 2014; Vardabasso et al., 2015), BRD2 is preferentially enriched at promoters compared to enhancers, while BRD4 is enriched at SEs and SE-associated gene promoters (Figures 5B, 5C, and S5E).

Our BRD4 analysis further revealed that melanoma-associated genes such as *LIF*, *CCND1*, and *BRD2* (Kuphal et al., 2013; Vardabasso et al., 2015; Vízkeleti et al., 2012) have putative SEs (Figure 5A). *AMIGO2* was associated with two SEs, and three other genes from the proliferation mini-screen (*HMGA2*, *ZBTB38*, and *PDGFC*) (Figure 1E) were also associated with SEs (Figures 5A, S5B, and S5F). Other genes from the mini-screen, including *FST*, *ZIC1*, and *TBX18* (Figure 1E), were associated with TEs (Figures 5A, S5B, and S5F).

BETi Displaces BRD4 and BRD2 from SEs and Associated Promoters

To gain mechanistic insight into melanoma BETi sensitivity, we investigated changes in BET occupancy at TEs, SEs, and associated genes upon BETi treatment in SKmel147 cells treated with JQ1 for 6 hr. Upon BET inhibition, we observed depletion of BRD2 and BRD4 from TEs and SEs and, to a lesser extent, from TE/SE-associated promoters (Figures 5B, 5C, S5E, and S5F), correlating with decreased expression of TE/SE-associated genes (Figure 5D). Two BETi-sensitive genes from the mini-screen were not associated with a TE or SE (*MED25* and *REXO1*), suggesting their sensitivity is conferred by BET displacement from their promoters (Figure S5F). Collectively, these data suggest that BRD2 and BRD4 occupancy at both promoters and/or enhancers is important for gene activation and that BRD2 and BRD4 eviction from these regulatory elements plays a key role in regulating BETi sensitivity in a locus-specific manner.

Melanoma SEs Are Absent in NHMs and Are Heterogeneous across Cell Lines

To investigate whether the identified SEs were associated with melanocytic transformation, we examined the melanoma SEs in NHMs. While NHMs and melanoma cells displayed comparable levels of BRD2 and BRD4 genome-wide (Figure S5G), the majority of

melanoma SEs, TEs, and associated gene promoters were depleted of BRD2 and BRD4 in NHM (Figures 5E, S5F, and S5H). Using Assay for Transposase-Accessible Chromatin (ATAC)-seq (Buenrostro et al., 2013) and ChIP-seq for H3K4me1 and H3K27ac (Creyghton et al., 2010), we identified ~1,400 constituent enhancers within the SEs of melanoma cells (Table S5) and found them largely devoid of open chromatin, H3K27ac, and H3K4me1 in NHMs (Figures 5F and 5G). Together, this suggests that the transformation of NHMs to melanoma involves the reorganization of the enhancer landscape to promote melanoma gene expression programs.

To investigate enhancer heterogeneity in melanoma, we expanded our analysis to additional cell lines, including 501MEL, SKmel239 ($BRAF^{V600E}$), and SKmel2 ($NRAS^{Q61R}$), and an additional NHM line. This analysis showed H3K27ac and H3K4me1 heterogeneity among melanoma cell lines and more so compared to NHMs (Figure S6A). Using distance correlation, we classified NHM and melanoma cell lines based on their H3K27ac levels at enhancer regions (Figure S6A) and found that NHMs cluster together, yet separately from melanoma (Figure S6B). Surprisingly, melanoma lines clustered based on their mutation status for H3K27ac levels within SEs and for expression of their associated genes (Figure S6B).

Melanoma SEs Are Regulated by AP1 and TEAD TFs

We next performed motif analysis on the top 150 SEs (Figure 5B) and identified JUN and FOSL1/2 (of the AP-1 TF complex), TEAD1/4, and TGIF1/2 (Figure 5H), all of which have been implicated in melanoma or other cancers (Agrawal et al., 2017; Ozanne et al., 2007; Verfaillie et al., 2015; Xiang et al., 2015). ChIP-seq analysis showed FOSL2 and TEAD4 enrichment at melanoma SEs and TEs (Figures 5I and S6C). We further found the promoters and TEs/SEs of FOSL1/2 and TEAD1/4 themselves to be BET bound (Figures 5A and S6D; Table S5), yet without changes in their expression levels or BET occupancy upon JQ1 treatment (Figures S6D, and S6E; Table S1), suggesting these TFs may be insensitive to BETi.

AMIGO2 Is Regulated by BETs and AP1/TEAD TFs

We identified two putative active SEs upstream of the *AMIGO2* TSS (~20 kb and ~200 kb) in SKmel147 cells (Figure 6A). Interestingly, *AMIGO2* and its SEs are located within the same putative topologically associating domain (TAD) (Dekker and Heard, 2015) and lamina-associated domain (Fu et al., 2015), as suggested by flanking H3K27me3, macroH2A1, and macroH2A2 repressive domains, respectively, as well as CTCF occupancy (Hanssen et al., 2017) (Figure 6A). This region also contains *PCED1B*, which is not expressed (Table S1) and therefore unlikely to be regulated by these SEs.

We focused on the SE immediately upstream of *AMIGO2* due to its presence across multiple melanoma lines (while it is largely absent from NHMs) (Figure 6B). Moreover, we found this SE in an additional panel of melanoma cell lines and STCs using published H3K27ac ChIP-seq data (Kaufman et al., 2016; Verfaillie et al., 2015) (Figure 6C). This suggests that *AMIGO2* regulation through this SE is conserved across melanomas independent of

mutational status and despite SE heterogeneity (Figures S6A and S6B). Additionally, *AMIGO2* expression significantly correlates with H3K27ac levels at this SE (Figure 6D).

To further dissect the contribution of BET proteins to *AMIGO2* expression and its sensitivity to BETi, we assessed *AMIGO2* expression changes upon individual BET knockdown. We observed that BRD2 and BRD4 silencing, but not BRD3 silencing, suppressed *AMIGO2* (Figure 6E). Moreover, the *AMIGO2* locus and its SEs are enriched for BRD2 and BRD4 in melanoma compared to NHM and depleted upon BETi treatment (Figures 6F and S6F).

Based on our ATAC-seq and ChIP-seq data in SKmel147 cells, we identified five constituent enhancers (E1–E5) within the *AMIGO2* SE (Figures 6B and 6F), which were bound by FOSL2 and TEAD4 (Figure 6G). Interestingly, E1–E3 were shared between most melanoma lines, and E4 and E5 were predominant in SKmel147 cells (Figures 6B and 6C), in accordance with its higher *AMIGO2* levels (Figures 2A and 6D). To determine whether these TFs play a functional role in melanoma and in *AMIGO2* regulation, we knocked down FOSL2 and TEAD4/1 in SKmel147 cells (Figures 6H and S6G). Because the TEAD family members can function in a redundant manner (Verfaillie et al., 2015), we silenced TEAD4 and TEAD1 simultaneously (Figure S6G). FOSL2 and TEAD4/1 knockdown significantly abrogated melanoma growth (Figure S6H) and suppressed *AMIGO2* (Figures 6H and S6G). Thus, *AMIGO2* expression in melanoma and its sensitivity to BETi likely occurs via the action of BETs and the above TFs.

AMIGO2 Expression Is Controlled by Its Upstream SE

To test the functionality of the predicted enhancers (Figures 6B and 7A), we cloned E1–E5 upstream of a minimal promoter driving luciferase expression (Prescott et al., 2015) and trans-fected these constructs into SKmel147 cells. All enhancers, except E1, promoted transcriptional activity (Figures 7B and S7A). We next used CRISPR/Cas9 editing to individually delete the genomic regions containing E2–E3 and E4–E5 (Figures 7A, S7B, and S7C). These deletions suppress *AMIGO2* expression relative to a non-edited control (Figure 7C). Moreover, using a proliferation competition assay, we observed that deletion of either E2–E3 or E4–E5 confers a growth disadvantage for melanoma cells (Figure S7D). Finally, to confirm the contribution of FOSL2 and TEADs to *AMIGO2* expression through its SE, we deleted their DNA motifs within E3. We first divided the enhancer into three segments, E3A–C (Figure 7A, top), and found E3's activity largely encoded by E3A (Figure 7D). Deletion of the FOSL2 and TEAD4/1 motifs within E3A significantly diminished its activity (Figure 7D). Collectively, our data confirm that the proximal upstream SE controls *AMIGO2* expression in melanoma.

DISCUSSION

Based on the hypothesis that BET proteins orchestrate a transcriptional program that supports melanoma growth, we utilized BET inhibition to identify essential genes in malignant melanoma. We then selected a subset of uncharacterized BETi-sensitive genes that are upregulated in melanoma versus NHM and assessed their contribution to proliferation. We focused on *AMIGO2*, which encodes a transmembrane protein, and

demonstrated a pro-survival role for AMIGO2 in melanoma cells, independent of the driver mutations they harbor.

AMIGO2 is a member of the Amphoterin-induced gene and ORF family and shares similar structure with AMIGO1 and AMIGO3 (Kuja-Panula et al., 2003). Their extracellular domains contain six LRRs flanked by cysteine-rich domains and an Ig-like domain, and the cytosolic regions contain serines and thre-onines that potentially transduce signaling cues (Rabenau et al., 2004). AMIGO proteins were discovered in a screen for genes that control adhesion processes necessary for axon extension and fasciculation (Kuja-Panula et al., 2003). AMIGO2 was independently identified as pro-survival factor of cerebellar granule neurons upon depolarization (Ono et al., 2003). Recently, AMIGO2 was reported as a pro-survival factor in endothelial cells subjected to hypoxia, thus playing a key role in the vasculature (Park et al., 2015).

Here, we find the kinase-dead receptor PTK7 to interact with AMIGO2 at the membrane. We further showed that AMIGO2 modulation of PTK7 and its cleaved forms regulates melanoma cell survival, independent of the PI3K/AKT and MAPK signaling pathways. Thus, the AMIGO2-PTK7 axis has emerged as a regulator of melanoma survival and an attractive therapeutic target. Interestingly, antibody-drug conjugates against PTK7 have been successfully tested in phase I clinical trials for solid tumors (Damelin et al., 2017), supporting the development of high-affinity monoclonal antibodies that block the AMIGO2-PTK7 interaction with possible therapeutic efficacy in melanoma.

To comprehend the pro-tumorigenic transcriptional programs of melanoma and the mechanisms by which BET perturbation impacts gene expression programs, we mapped the enhancer landscape of NHMs and melanoma cells. We find that the transformation of NHMs to melanoma involves a significant reorganization of enhancer elements, and that a large number of SE-regulated genes are associated with cancer, as previously proposed (Roe et al., 2015). Our data suggest that using BRD4 enrichment to identify SE-regulated genes may be useful for identifying melanoma driver genes. Genome-wide studies of BRD2 revealed that, akin to BRD4, it is enriched at TEs and SEs. However, unlike BRD4, BRD2 preferentially binds promoter regions and CTCF-occupied regions (data not shown) (Hsu et al., 2017), suggesting distinct yet cooperative roles in transcriptional regulation.

Following BET inhibition, we observed differential genome-wide displacement of BRD2 and BRD4 from TEs, SEs, and the promoters of their associated genes, which correlates with reduced expression of JQ1-sensitive genes. Our data suggest, however, that BETi sensitivity is not restricted to genes that are associated with BET-occupied enhancers. BETi sensitivity can also occur through BRD2 and BRD4 eviction from promoters. We also highlight that not all BET-occupied genes are necessarily BETi sensitive, the reasons for which remain unclear, but may involve chromatin architecture or mRNA stability.

As suggested for other cancers (Akhtar-Zaidi et al., 2012; Ooi et al., 2016), we observed enhancer variation across melanomas. Despite this heterogeneity, we find the *AMIGO2* SE to be present in all melanoma cells studied and inactive in NHMs largely through the lack of BET proteins and H3K27ac. We speculate that during transformation, this SE is activated,

followed by acquisition of BRD2, BRD4 and FOSL and TEAD TFs (see model, Figures 7E and 7F). Upon BETi treatment, BET displacement from the *AMIGO2* SEs and promoter allows transcriptional downregulation (Figures 7E and 7F). However, it remains unclear whether these particular TFs are displaced by BET inhibition and how BET proteins and TFs functionally cooperate at the *AMIGO2* SEs.

Our understanding of AMIGO2 function in cancer has been limited (Kanda et al., 2017; Park et al., 2015), likely due to the lack of evidence for genetic alterations. Here, we report that AMIGO2 is required for melanoma cell proliferation and survival and is induced by the acquisition of active *cis* DNA regulatory elements absent in NHMs. Ongoing studies will further illuminate AMIGO2 function in cancer and inspire the development of small-molecule inhibitors or antibodies against this transmembrane protein and/or its partner, PTK7.

STAR★METHODS

Detailed methods are provided in the online version of this paper and include the following:

KEY RESOURCES TABLE

REAGENT or RESOURCE	SOURCE	IDENTIFIER
Antibodies		
BRD2	Bethyl Laboratories	A302-583A
BRD4	Bethyl Laboratories	A301-985A
H3K4me1	Abcam	ab8895
H3K4me3	Abcam	ab1012
H3K27ac	Abcam	ab177178
H3K27me3	EMD	07-449
MED1	Bethyl Laboratories	A300-793A
macroH2A2	Bernstein Laboratory, ISMMS	in house
macroH2A1	Abcam	ab37264
CTCF	EMD	07-729
FOSL2	Santa Cruz	SC-604
TEAD4	Santa Cruz	SC-101184
HSP90	Santa Cruz	SC-13119
GAPDH	Santa Cruz	SC-32233
GFP	Roche	11814460001
LAMIN B1	Santa Cruz	SC-6217
ALCAM	Abcam	ab109215
L1CAM	Abcam	ab20148
NRP2	Santa Cruz	SC-13117
NRP1	Abcam	ab81321
TUBULIN	Sigma	T9026

REAGENT or RESOURCE	SOURCE	IDENTIFIER
FOXM1	Cell Signaling Technology	5436
Casp3	Cell Signaling Technology	9662
PARP	Cell Signaling Technology	9542
AMIGO2 (for IHC)	Abnova	H00347902-B01P Lot# F8271 RRID:AB_1672842
AMIGO2 (for IF and WB)	R&D systems	AF2080
PTK7 (N-terminal) (for WB)	R&D systems	AF4499
PTK7 (C-terminal) (for IF and WB)	Cell Signaling	11926
Secondary rabbit anti goat (for AMIGO2 detection on WB)	Sigma	A5420
HRP-conjugated ACTIN	Sigma	A3854
Biological Samples		
Melanoma and normal skin tissue microarray	Biomax	ME208
Nevus tissue microarray	IMCG, NYU	MT032808
Patient derived short term cultures	Osman Laboratory, NYU	de Miera et al., 2012
NHM (this paper)	Bernstein Laboratory, ISMMS	NHM1-5
Chemicals, Peptides, and Recombinant Proteins		
GFP Trap-A beads	Chromotek	gta-10
BET inhibitor JQ1	Bradner Laboratory; Agreement #A09608	N/A
BET inhibitor I-BET762	Apex Bio	501014747
IGEPAL	Sigma	I-8896
Micrococcal Nuclease	Affymetrix	70196Y
Dynabeads Protein A Immunoprécipitation kit	Invitrogen	10006D
Magna ChIP Protein A+G Magnetic beads	Millipore	16-663
DSG	Pierce (ThermoFisher)	20593
Critical Commercial Assays		
Click- Click-IT EdU Pacific Blue Flow Cytometry Assay Kit	ThermoFisher	C10636
Caspase Activity assay	MBL Int. Corporation	BV-1007-13
AnnexinV Pacific Blue	BioLegend	640918
Nextera DNA Library Preparation Kit	Illumina	FC-121-1030
Ribo-Zero Gold Kit	Illumina	MRZG12324
BLOCK-iT Fluorescent Oligo	Invitrogen	2013
RNeasy QIAGEN extraction kit	QIAGEN	74104
OneStep PCR Inhibitor Removal columns	ZYMORESEARCH	D6030
QIAGEN miRNeasy minikit	QIAGEN	217004
Ribo-Zero rRNA Removal kit	Illumina	MRZH116
ScriptSeq Complete Gold kit	Illumina	BEP1206

REAGENT or RESOURCE	SOURCE	IDENTIFIER
TOPO TA Cloning Kit for Sequencing	Invitrogen	45-0030
Deposited Data		
Raw and analyzed RNA sequencing, ATAC-seq and ChIP-sequencing data	See Table S6	GSE94488
Complete immunoblot images and AMIGO2 pull down mass spectrometry data	See Table S4 and Mendeley Data	https://doi.org/10.17632/8g4vcy4ymm.1
RNA-sequencing data of human primary and metastatic melanoma	TCGA	Cancer Genome Atlas, 2015
Expression array data of human primary and metastatic melanoma	Xu et al., 2008	GSE8401
Experimental Models: Cell Lines		
501MEL	Yale University	N/A
SKmel147	MSKCC	N/A
SKmel2	ATCC	HTB-68
SKmel28	ATCC	HTB-72
SKmel239	MSKCC	N/A
SKmel94	MSKCC	N/A
SKmel197	MSKCC	N/A
SKmel100	MSKCC	N/A
SKmel173	MSKCC	N/A
SKmel29	MSKCC	N/A
SKmel103	MSKCC	N/A
A375	ATCC	CRL-1619
SKmel192	MSKCC	N/A
SKmel5	ATCC	HTB-70
SKmel187	MSKCC	N/A
WM278	Osman Laboratory, NYU	N/A
WM1361A	Osman Laboratory, NYU	N/A
451Lu	Osman Laboratory, NYU	N/A
MeWo	ATCC	HTB-65
Experimental Models: Organisms/Strains		
Mouse: female, 6 to 8 weeks old, NOD/SCID/IL2$\gamma R^{-/-}$	Jackson Laboratories	05557
Oligonucleotides		
Primers for AMIGO2, BRD4, BRD2, BRD3, HMGA2, MED25, ZIC1, ZBTB38, PPIA, GAPDH, TEAD1, TEAD4	Table S7	N/A
siRNA ON-target plus SMARTpool BRD2	Dharmacon	L-004935
siRNA ON-target plus SMARTpool BRD3	Dharmacon	L-004936
siRNA ON-target plus SMARTpool BRD4	Dharmacon	L-004937

REAGENT or RESOURCE	SOURCE	IDENTIFIER
siRNA ON-target plus SMARTpool AMIGO2	Dharmacon	L-018701
siRNA ON-target plus SMARTpool ZIC1	Dharmacon	L-011798
siRNA ON-target plus SMARTpool HGMA2	Dharmacon	L-013495
siRNA ON-target plus SMARTpool MED25	Dharmacon	L-014689
siRNA ON-target plus SMARTpool ZBTB38	Dharmacon	L-023605
siRNA ON-target plus SMARTpool PDGFC	Dharmacon	L-013154
siRNA ON-target plus SMARTpool TBX18	Dharmacon	L-024872
siRNA ON-target plus SMARTpool REXO1	Dharmacon	L-021445
siRNA ON-target plus SMARTpool FST	Dharmacon	L-012221
siRNA ON-target plus SMARTpool NTC	Dharmacon	D-001810-10-05
Recombinant DNA		
plkO.1-human-shAMIGO2 #1	Sigma-Aldrich	TRCN0000160033
plkO.1-human-shAMIGO2 #2	Sigma-Aldrich	TRCN0000159658
plkO.1-human-shAMIGO2 #3	Sigma-Aldrich	TRCN0000162315
plkO.1-human-shAMIGO2 #4	Sigma-Aldrich	TRCN0000158754
Plenti-Cas9-Blast	Addgene	52962
pGL3-noSV40	Wysocka Laboratory	Prescott et al., 2015
pLenti-CMV-AMIGO2-GFP-Puro	This paper	N/A
pLenti-CMV-GFP-Puro	Addgene	17448
pSPAX2	Addgene	12260
pMD2.G	Addgene	12259
plkO.1-human-shFOSL2 #1	Sigma-Aldrich	TRCN0000329767
plkO.1-human-shFOSL2 #2	Sigma-Aldrich	TRCN0000016138
plkO.1-human-shTEAD4 #1	Sigma-Aldrich	TRCN0000285156
plkO.1-human-shTEAD4 #2	Sigma-Aldrich	TRCN0000015877
plkO.1-human-shTEAD1 #1	Sigma-Aldrich	TRCN0000278040
plkO.1-human-shSCR	Dharmacon	RHS6848
pLenti-Cas9-Blast	Addgene	52962
Human AMIGO2 cDNA	Dharmacon	pBluescript, MHS6278-202804749
pLenti-GFP/mCherry	Brown Laboratory, ISMMS	N/A
Software and Algorithms		
Bowtie	version 0.12.7	N/A
Bowtie2	version 2.1.0	N/A
Samtools	version 0.1.19	N/A
BedTools	version 2.17.0	N/A
deepTools	version 2.4.1	N/A

REAGENT or RESOURCE	SOURCE	IDENTIFIER
HOMER	version 4.8	N/A
RStudio	version 0.99.491	N/A
Cufflinks	version 2.1.1	N/A
MACS2	version 2.1.1.2	N/A
cuffdiff	version 2.1.1	N/A
TopHat	version 2.1.0	N/A
ROSE	ROSE	N/A
Enrichr	Enrichr	N/A
GEDI	version 2.1	N/A
NGS-QC	ngs-qc	N/A
RStudio	version 0.99.491	N/A
FLOWJO	version 8.7	N/A
Cluster 3.0	version 1.52	N/A
Java TreeView	version 1.1.6r4	N/A

CONTACT FOR REAGENT AND RESOURCE SHARING

Further information and requests for resources and reagents should be directed to and will be fulfilled by the Lead Contact, Emily Bernstein (emily.bernstein@mssm.edu).

EXPERIMENTAL MODELS AND SUBJECT DETAILS

Cell culture—501MEL (Female), SKmel147 (Female), SKmel2 (N/A), SKmel28 (N/A), SKmel239 (Female), SKmel197 (N/A), SKmel94 (N/A), SKmel100 (N/A), SKmel173 (N/A), SKmel29 (Male), SKmel103 (N/A), A375 (Female), SKmel192 (N/A), SKmel5 (Female) and SKmel187 (N/A) were grown in DMEM supplemented with 10% FBS, penicillin and streptomycin. Low passage melanoma short-term cultures (STCs), WM793B (Male), WM278 (Female), WM1361A (Male) and 451Lu (Male), a kind gift of the Osman laboratory, NYU, were grown in MCDB 153 supplemented with 10% FBS, penicillin and streptomycin (de Miera et al., 2012). MeWO (Male) were grown in EMEM supplemented with 10% FBS, penicillin and streptomycin. Normal human melanocytes (NHM1-5) were extracted and cultured as follows: Neonatal foreskins were collected in PBS, 1:100 Anti-Anti (100X Antibiotic-Antimycotic (GIBCO, Cat# 15240-062)), and kept at 4°C for no longer than 48 hr. Skins were then washed once in 70% EtOH and 3x in PBS, 1:100 Anti-Anti, cut into 3-4 pieces in HBSS (GIBCO, Cat# 24020-117) and placed in Dispase II solution (Roche, Cat# 04942078001) at 4°C O/N. Epidermis then separated from the dermis in HBSS, floated in 1 mL of 0.25% trypsin (GIBCO, Cat# 15400-054), and incubated in 37°C for 3 min with agitation. Cells were then collected into 4 mL of DMEM with 10% FBS and spun at 1200 rpm for 5 min twice. Media was then removed from the first and the second cell pellets, which were then consolidated and resuspend in Melanocyte Growth Media 254 supplemented with Human Melanocyte Growth Supplement (HMGS, Life Technologies, Cat# S-016-5) and 0.2 μM $CaCl_2$, for 3-5 days. Cells were then rinsed in PBS, 1:100 Anti-Anti, and trypsinized in 1 mL 0.05% Trypsin for 3 min to separate melanocytes

from fibroblasts and keratinocytes, which take longer to detach. Cells were then collected into 4 mL of DMEM with 10% FBS, and spun at 1200 rpm for 5 min and resuspended and cultured in Melanocyte Growth Media 254 supplemented with HMGS, 0.2 μM $CaCl_2$, and 10 ng/mL PMA (Sigma, Cat# P8139).

Mice—NOD/SCID/IL2γR$^{-/-}$ female mice (Jackson labs, Cat# 05557) were used for *in vivo* studies. Experiments were conducted following protocols approved by the NYU Institutional Animal Care Use Committee (IACUC) (protocol number, S16-00051).

METHOD DETAILS

IC_{50} curves—Cells were seeded at 2×10^4 cells per well on a 96-well plate and treated with varying concentrations of JQ1 (JQ1(+)) for 72 hr. Cell viability was measured as described below and results were plotted relative to the lowest concentration.

Reverse transfection—Cells were seeded at 3×10^4 cells per well on a 96-well plate and transfected with Lipofectamine 2000 (Invitrogen) and siRNA ON-target plus SMARTpools for each of the indicated candidate genes and with siSCR control, at a final concentration of 20 nM (n = 3/siRNA). At 48 hr post-transfection, cells were seeded for cell proliferation screens.

Cell viability assays—Transfected, transduced or JQ1-treated cells were seeded at 3×10^3 or 2×10^3 cells per well in 96 well plates. The following day (day 0) and every 24 hr after (up to 4 days), cells were fixed in 0.1% glutaraldehyde and stored in PBS at 4°C. Cells were then stained with 0.5% crystal violet, dissolved with 15% acetic acid. Optical density was read at 590nm. For normalization and control purposes, cells transfected, transduced with non-targeting scramble controls (siSCR) were present on each experiment. Viability data are relative to the siSCR-transfected cells.

Colony formation assay—Cells were seeded at 1×10^3 cells per well on a 6-well plate (n = 2/condition) and media was changed every 3 days. Fourteen days post-seeding, cells were fixed in 0.1% glutaraldehyde and 0.5% crystal violet. After washing off excess crystal violet, plates were scanned and colony number was manually assessed.

Plasmids, lentiviral vector production and cell transfection—To generate AMIGO2-GFP, the human AMIGO2 cDNA was purchased from Dharmacon (pBluescript, MHS6278-202804749) and subcloned into the pLenti-CMV-GFP-Puro vector (Addgene, Cat# 17448) using XbaI (5′-GCGGATCCGCagtggacgccacaaaaggtgtgtcagaaaa-3′) and BamHI (5′-CTAGTCTAGAATGTCGTTACGTGTACACACTCTGCCCACCCT-3′). For lentiviral vectors production HEK293T cells were seeded in 10 cm tissue culture dish and incubated at 37°C and 5% CO_2. When cells reached 80% confluency they were co-transfected with 12 μg of lentiviral expression constructs, 8 μg of psPAX2 and 4 μg pMD2.G vectors using Lipofectamine 2000 (Invitrogen) following manufacturer's recommendations. At 48 hr post transfection supernatants were collected, filtered (0.45 μm) and stored at −80°C (Segura et al., 2013). Melanoma cells were infected with lentiviral supernatant supplemented with polybrene at a final concentration of 4 μg/mL. siRNA ON-target plus

SMARTpools were purchased from Dharmacon. 50 nM of the corresponding siRNA were transfected using Lipofectamine 2000 (Invitrogen) following manufacturer's protocol. Transfection efficiency was monitored using 50 nM BLOCK-iT Fluorescent Oligo (Invitrogen).

RNA extraction, Reverse Transcription and qRT-PCR—Total RNA was extracted using RNeasy QIAGEN extraction kit according to the manufacturer's protocol. 1 μg of RNA was subjected to DNase I treatment and reverse transcription. Real-time PCR of the gene of interest was performed using SYBR green (Applied Biosystems or Roche). Expression levels are shown relative to *PPIA* or *GAPDH* as indicated. For NHM, RNA was further purified using OneStep PCR Inhibitor Removal columns (ZYMORESEARCH, Cat# D6030) to remove melanin prior to qRT-PCR.

Flow cytometry, apoptosis, and cell cycle analysis—Cells were seeded at 1.5×10^5 cells per well on 6-well plates (n = 2/condition). For apoptosis measurements, non-adherent and adherent cells were collected and stained with AnnexinV-Pacific Blue (BioLegend, Cat# 640917) and PI, following manufacturer's protocol. For cell cycle analysis, cells were pulsed with EdU (ThermoFisher, Click-IT EdU Pacific Blue Flow Cytometry Assay Kit) for 1 hr, brought to suspension and fixed following manufacturer's protocol. Pulsed cells were co-stained with PI at a final concentration of 10 μg/mL. A BD LSRII cytometer was used for data acquisition and Flowjo software for analysis.

Caspase activity assay—Cells were treated with or without a pan-caspase inhibitor (10 nM, QVD) 24 hr post-lentiviral infection. Cells were then rinsed 1x with PBS and resuspended in 1X lysis buffer (20 mM HEPES/NaOH, pH 7.2, 10% sucrose, 150 mM NaCl, 10 mM DTT, 5 mM EDTA, 1% Igepal CA-630, 0.1% CHAPS, and 1X EDTA-free Complete protease inhibitor mixture (Roche)). Lysates were cleared by centrifugation at 16,000×*g* for 5 min and supernatants quantified by the Lowry method (Bio-Rad). Assays were performed in triplicate using 25 μg of protein in lysis buffer supplemented with 25 μM of the fluorogenic substrate Ac-DEVD-afc. Plates were read in a fluorimeter using a 400 nm excitation filter and a 505 nm emission filter.

Whole cell protein extractions and western blot analysis—Cells were harvested with PathScan Sandwich ELISA 1X lysis buffer (Cell Signaling Cat# 7018) supplemented with protease and phosphatase inhibitor cocktail (Roche). Cell lysates (15-40 μg of protein) were resolved in 4%–12% Bis-Tris gels (Invitrogen) and transferred to nitrocellulose membranes using semi-dry transfer. After blocking (1 hr to overnight with 5% nonfat milk), membranes were probed with primary antibodies overnight at 4°C. Membranes were developed using Clarity western ECL blotting substance (Biorad, Cat# 1705060). For AMIGO2, primary antibody was used at 1:100 (R&D systems). Secondary detection was performed using rabbit anti-goat at 1:20,000 (Sigma, Cat# A5420). Immunoblots were done on whole-cell lysates unless otherwise indicated.

Immunohistochemistry (IHC)—Unconjugated anti-human AMIGO2, raised against full-length human AMIGO2 was used for IHC. Antibody optimization was performed on formalin-fixed, paraffin-embedded 4-micron composite tissue microarrays containing

normal and tumor: skin, stomach, prostate, liver, and pancreas. IHC parameters were validated on formalin-fixed, paraffin-embedded 4-micron human hippocampus with cells clearly expressing cytoplasmic-membrane staining considered positive. Chromogenic IHC was performed on a Ventana Medical Systems Discovery XT instrument with online deparaffinization using Ventana's reagents and detection kits unless otherwise noted (Ventana Medical Systems Tucson, AZ USA). AMIGO2 was antigen-retrieved in Ventana Cell Conditioner 1 (Tris-Borate-EDTA) for 20 min. Antibody was diluted 1:50 in PBS and incubated for 6 hr at room temperature. Primary antibody was detected with goat anti-mouse, horseradish peroxidase conjugated multimer incubated for 8 min. The complex was visualized with alpha-naphthol pyronin incubated for 8 min. Slides were washed in distilled water, counterstained with Hematoxylin, dehydrated and mounted with permanent media. Negative controls were incubated with diluent instead of primary antibody. Staining score was performed in a blinded manner. The IHC score was calculated using staining intensity (1-4) × percentage of positive cells.

Immunofluorescence—SKmel147 cells were grown on glass coverslips (SKmel147 cells stably expressing AMIGO2-GFP were used in Figure 4A), fixed in 4% PFA for 15 min and permeabilized with 100 μM saponin for 30 min. Primary antibodies were used at the following dilutions: AMIGO2 1:500 (Figure 4A), and AMIGO2 1:200 and PTK7 1:200 (Figure S4C). Secondary detection was performed using Alexa Fluor conjugated antibodies diluted 1:1000, nuclei were counterstained with Hoechst 33342 and coverslips were mounted in ProLong Diamond Antifade (ThermoFisher). Images were acquired on a LSM 780 confocal microscope controlled by ZEN software (Carl Zeiss) using a 40× immersion objective, 2× internal magnification and optimal voxel size. Single Z slices are shown.

Affinity purification and mass spectrometry (MS) analysis—SKmel147 cells stably expressing AMIGO2-GFP or GFP were fixed with 1% formaldehyde for 10 min at RT. Fixing reaction was quenched with 2.5 μM glycine. Whole cell extracts were harvested with 1X lysis buffer (10 mM Tris pH 7.5, 150 mM NaCl, 0.5 mM EDTA, 0.5% NP-40) supplemented with phospatase and protease inhibitors (Roche). 1 mg of protein was incubated with 25 μL of washed beads O/N, washed 3x with wash buffer (1 mM Tris pH 7.5, 150 mM NaCl, 0.1% NP-40, supplemented with phosphatase and protease inhibitors), and eluted in 2X sample buffer. Samples were then run on NuPAGE 4%–12% Bis-Tris Gel 1.0 mm (Life Technologies) and desired fractions were extracted and subsequently digested with trypsin. Peptides were extracted using Poros beads (Life Technologies) for MS analysis. LC separation was conducted with the auto sampler of an EASY-nLC 1000 (ThermoFisher). Peptides were gradient eluted from the column directly to QExactive mass spectrometer using a 90 min gradient (ThermoFisher). For identification of AMIGO2 unique interactors, we determined the peptides uniquely found in AMIGO2-GFP pull downs versus GFP (n = 3). We then filtered out potential contaminants using a contaminant repository (CRAPome (Mellacheruvu et al., 2013)) with a threshold of > 3/411 (Table S5).

Mouse experiments—SKmel147 cells were infected with shSCR or sh*AMIGO2* lentivirus (shA2 #2) for 2 days and then injected at 5×10^5 cells per mouse in the flanks of

female NOD/SCID/IL2γR$^{-/-}$ mice (n = 8/group). Tumor volume was measured every 2-3 days over a period of 18 days and tumor weight was measured at endpoints.

Reverse phase protein array (RPPA)—501MEL and SKmel147 cells where transfected with shSCR or sh*AMIGO2* (shA2 #2) and 48 hr post-transfection protein extracts where collected as follows: cells were washed 2x with cold PBS and incubated for 20 min on ice with 1X lysis buffer (1% Triton X-100, 50 mM HEPES, pH 7.4, 150 mM NaCl, 1.5 mM $MgCl_2$, 1 mM EGTA, 100 mM NaF, 10 mM Na-pyrophosphate, 1 mM Na_3VO_4, 10% glycerol, with freshly added phosphatase and protease inhibitors (Roche)). Lysates were cleared by centrifugation at 14,000×*g* for 5 min, and supernatants were quantified by the Lowry method (Bio-Rad). Samples were diluted with 4X SDS sample buffer (40% Glycerol, 8% SDS, 0.25 M Tris pH 6.8, supplemented with fresh 2-mercaptoethanol). Equal amounts of proteins per sample were loaded onto the array (Park et al., 2010). Unpaired Student's t test was performed to determine statistically significant changes ($p < 0.05$) between shSCR and shA2 #2. Heatmaps for significant changes (Figure S3B, S3D) were generated using Cluster 3.0 and Java TreeView.

RNA-sequencing—Total RNA was extracted from two NHM cultures, SKmel2, SKmel239, SKmel147 and 501MEL melanoma cell lines treated with enan-tiomer (JQ1[−]) or 10 μM JQ1 (JQ1(+)) for 6 or 24 hr, in technical replicates. RNA was extracted using QIAGEN miRNeasy minikit. RNA was then processed with Ribo-Zero rRNA Removal Kit (Illumina) to remove rRNA, and further processed into sequencing libraries using Illumina ScriptSeq Complete Gold kit, following manufacturer's protocol. All libraries were sequenced on Illumina HiSeq2500 (~150M, 50bp paired-end). Reads were aligned to the GRCh37/hg19 using TopHat (version 2.1.0) (Trapnell et al., 2012). Normalized transcriptome assemblies in FPKM, and differential expression ratios were computed with Cufflinks (version 2.1.1) (Trapnell et al., 2012). Coverage tracks were generated using deepTools (version 2.4.1) with parameters bamCoverage –normalizeUsingRPKM –bin-size 10 (Ramírez et al., 2014). In all samples, genes were called 'expressed' if normalized FPKM ≥ 1.5. Genes were called downregulated upon JQ1 treatment if FPKM ≥ 1.5; log2FoldChange ≤ −0.625; and Padj < 0.05. Genes were called overexpressed over NHM if nFPKM ≥ 1.5 (in the melanoma sample); log2FoldChange ≥ 2; and Padj < 0.05. Genes were called downregulated upon AMIGO2 depletion if FPKM ≥ 1.5 (prior to depletion); log2FoldChange ≤ −1.2; and Padj < 0.05. log2FoldChange ≥ 1.2 for upregulated genes. Scatterplots were generated using R (gplots). Volcano plots were generated using R (CummeRbund). Heatmap for 78 putative pro-tumorigenic genes (Figure 1D) was generated using R (ggplot2). All FPKM values are normalized.

Native and crosslinked ChIP and next-generation sequencing—For native ChIP (H3K4me3, H3K4me1, H3K27ac, macroH2A1, macroH2A2 and H3K27me3), 3–4×10^7 cells were collected and resuspended in 2 mL of ice cold buffer I (0.32 M Sucrose, 60 mM KCl, 15 mM NaCl, 5 mM $MgCl_2$, 0.1 mM EGTA, 15 mM Tris pH 7.5, 0.5 mM DTT, 0.1 mM PMSF, 1:1000 protease inhibitor cocktail). 2 mL of ice-cold buffer I supplemented with 0.05%–0.2% IGEPAL (Sigma) was then added. The resulting 4 mL of nuclei was placed on ice for 10 min and then gently layered on top of 8 mL of ice-cold buffer III (1.2 M Sucrose,

60 mM KCl, 15 mM NaCl, 5 mM $MgCl_2$, 0.1 mM EGTA, 15 mM Tris pH 7.5, 0.5 mM DTT, 0.1 mM PMSF, 1:1000 protease inhibitor cocktail) and centrifuged at 10,000×g for 20 min at 4°C with no brake. Pelleted nuclei were resuspended in 200 μL buffer A (0.34 M sucrose, 15 mM HEPES pH 7.4, 15 mM NaCl, 60 mM KCl, 4 mM $MgCl_2$, 1 mM DTT, 0.1 mM PMSF, 1:1000 protease inhibitor cocktail) and further diluted to 600 ng/μL. MNase (Affymetrix) digestion reactions were carried out on 100 μg or more chromatin using 0.05–0.2 U/μg chromatin in buffer A supplemented with 3 mM $CaCl_2$, 1 mM DTT, 0.1 mM PMSF and 1:1000 protease inhibitor cocktail, for 10 min at 37°C. The reaction was quenched with 5 mM EGTA on ice and centrifuged at 13,500×g for 10 min at 4°C. The chromatin was resuspended in 10 mM EDTA pH 8.0, 1 mM DTT, 1 mM PMSF and 1:1000 protease inhibitor cocktail, and rotated at 4°C for 2 hr. The mixture was adjusted to 500 mM NaCl, allowed to rotate for another 45 min and then centrifuged at 13,500×g for 10 min yielding nucleosomes in the supernatant. 100 μg or more of chromatin was diluted to 100 ng/μL with buffer B (20 mM Tris pH 8.0, 5 mM EDTA, 500 mM NaCl, 0.2% Tween 20, 1 mM DTT, 1 mM PMSF, 1:1000 protease inhibitor cocktail) and pre-cleared with protein A (Invitrogen) or A+G (Millipore) magnetic beads pre-conjugated with rabbit or mouse IgG (15 μL slurry and 15 μg of IgG per 25 μg chromatin), for 2 hr at 4°C. 1–2 μg of the pre-cleared supernatant (bulk nucleosomes) was saved for further processing. To the remaining supernatant, pre-conjugated A or A+G magnetic beads;antibodies (10 μL slurry and 1 μg antibody per 10 μg chromatin) was added and rotated overnight at 4°C. Beads were washed 3x with buffer B, and 1x with buffer B without Tween, and DNA was eluted 2x in 100 μL fresh elution buffer (1% SDS, 100mM $NaHCO_3$) at 65°C for 30 min. For the input fraction, an equal volume of input recovery buffer (0.6 M NaCl, 20 mM EDTA, 20 mM Tris pH 7.5, 1% SDS) and 1 μL of RNase A (10 mg/mL) was added followed by incubation for 1 hr at 37°C. 100 μg/mL Proteinase K (ThermoFisher) was then added and was incubated for another 3 hr at 37°C. For the ChIP fraction, 12 μL of 5M NaCl and 1 μL of RNase A (10 mg/mL) was added followed by incubation for 1 hr at 37°C. 500 μg/mL Proteinase K (ThermoFisher) was then added and was incubated for another 3 hr at 37°C. Samples were then subjected to a phenol-chloroform extraction followed by purification using AMPure XP beads (Beckman Coulter, Cat# A63882). DNA was diluted to 4-6 ng/μL and run on an Agilent High Sensitivity DNA chip using Agilent Technologies 2100 Bioanalyzer (Hasson et al., 2013).

For BRD2, BRD4, MED1 and CTCF 72×10^6 cells (SKmel147 untreated (JQ1[−]) and treated with 10 μM JQ1 (JQ1(+)) for 6 hr, NHM untreated), were crosslinked with 1% PFA for 10 min at RT. The reaction was quenched with 0.125 M glycine for 5 min at RT and centrifuged at 1100 rpm for 3 min at 4°C. Cells were washed 1x in ice-cold PBS, resuspended at 18×10^6 in 500 μL ice-cold Cell Lysis Buffer (10 mM Tris pH 8, 10 mM NaCl, 0.2% NP-40, 1 mM PMSF, 1:1000 protease inhibitor cocktail) and incubated on ice for 15 min. Tubes were then centrifuged at 2K rpm for 5 min at 4°C, and pellets were resuspended in 500 μL ice-cold Nuclear Lysis Buffer (50 mM Tris pH 8, 10 mM EDTA, 1% SDS, 1 mM PMSF, 1:1000 protease inhibitor cocktail) and incubated on ice for 10 min. Sonication were carried out for 12-15 cycles, 30 s on, 30 s off, low intensity at 4°C in a Bioruptor sonicator (Diagenode). Chromatin was centrifuged at 13,000×g for 10 min at 4°C, consolidated and diluted 1:4 with IP Dilution buffer (20mM Tris pH 8, 2 mM EDTA, 150 mM NaCl, 1% Triton-X, 0.01% SDS, 1 mM PMSF, 1:1000 protease inhibitor cocktail).

Chromatin was pre-cleared with protein A (Invitrogen) or A+G (Millipore) magnetic beads pre-conjugated with rabbit or mouse IgG respectively (240 μL of slurry and 30 μg of IgG), for 2 hr at 4°C. 1–2 μg of the pre-cleared supernatant (bulk nucleosomes) was saved for further processing. To the remaining supernatant, pre-conjugated antibodies (240 μL slurry and 24 μg antibody) was added and rotated overnight at 4°C. Beads were washed 2x with ice-cold High Salt Buffer (20mM Tris pH 8, 2 mM EDTA, 500 mM NaCl, 1% Triton-X, 0.01% SDS, 1 mM PMSF, 1:1000 protease inhibitor cocktail), 1x with ice cold IP Wash I (20 mM Tris pH 8, 2 mM EDTA, 50 mM NaCl, 1% Triton-X, 0.1% SDS, 1 mM PMSF, 1:1000 protease inhibitor cocktail), 1x with ice-cold IP Wash II (10 mM Tris pH 8, 1 mM EDTA, 0.25 LiCl, 1% NP-40, 1% deoxycholic acid, 1 mM PMSF, 1:1000 protease inhibitor cocktail), and 2x with ice-cold TE (5 mM Tris pH 7.4, 1 mM EDTA). DNA was eluted as above (Roe et al., 2015). For TEAD4 and FOSL2, 7-9×10^6 cells (SKmel147 untreated), were washed 3x in PBS, 1 mM $MgCl_2$, crosslinked with 0.25M DSG (Pierce, Rockford IL) in PBS, 1 mM $MgCl_2$ for 45 min at RT, washed 3x in PBS, 1 mM $MgCl_2$, crosslinked in PBS, 1% PFA for 10 min at RT, washed 3x in PBS, and then harvested (Tian et al., 2012). Cells were processed and sonicated as above. ChIP reactions were carried out as above with 100 μL slurry and 10 μg antibody (Roe et al., 2015). Sequencing libraries were generated and barcoded for multiplexing according to Illumina recommendations with minor modifications. Briefly, 2–8 ng Input or ChIP DNA was end- repaired and A-tailed. Illumina Truseq adaptors were ligated, libraries were size-selected to exclude polynucleosomes, and the libraries were PCR-amplified using KAPA HiFi DNA Polymerase with no more than 12-15 cycles. All steps in library preparation were carried out using NEB enzymes (Hasson et al., 2013). Libraries were sequenced on Illumina Hi-Seq2500 or NextSeq500 (50-75bp single-end reads).

Reads were trimmed for Illumina adaptor sequences using in-house scripts and aligned to the GRCh37/hg19 using Bowtie (version 0.12.7) with parameters –l 40-65 –n 2 –S –best –k 1 –m 20/1, and further assessed for quality using NGS-QC (Langmead et al., 2009). Number of aligned reads for each sample is provided in Table S6. For BRD2, BRD4, TEAD4 and FOSL2 ChIP-seq, duplicate reads were removed before downstream analysis. BRD4 significant peaks in SKmel147 were identified using MACS2 (version 2.1.1.2) with parameters -s 100–nomodel —extsize 200 —slocal 1000 -q 0.01. H3K27ac significant peaks in SKmel147 were identified using with parameters–fe-cutoff 1.5 -s 100 -p 0.00001–nomodel–extsize 147–keep-dup 2. (Zhang et al., 2008). Matching Input control was used to call peaks. Coverage tracks were generated from BAM files using deepTools bamCoverage with parameters –normalizeU-singRPKM –binsize 10.

ATAC-seq—For all ATAC-seq libraries (Buenrostro et al., 2015), 150k cells were harvested, tagmented with 5uL Nextera Tn5 Transposes from Nextera kit (Illumina) for 30 min, amplified up to 10 cycles and then purified using QIAGEN MinElute columns (Buenrostro et al., 2013). Purified libraries were then size-selected on 2% agarose gel (150-700bp), followed by purification using AMPure XP beads (Beckman Coulter, Cat# A63882). DNA was diluted to 4-6 ng/μL and run on an Agilent High Sensitivity DNA chip using Agilent Technologies 2100 Bioanalyzer. Libraries were sequenced on Illumina Hi-Seq2500 (50bp paired-end reads). Reads were trimmed for Illumina adaptor sequences using

in-house scripts and aligned to the GRCh37/hg19 using Bowtie2 (version 2.1.0) with parameters –S –X 2000 (Langmead et al., 2009). Reads aligned to mtDNA, with quality value Q < 30, as well as duplicated reads, were removed using in-house scripts and Samtools. The final number of reads used to generate coverage tracks for each sample is provided in Table S6. Significant peaks were identified using MACS2 with parameters–nomodel–nolambada–keepdup all –slocal 10000. Coverage tracks were generated using deepTools bamCoverage with parameters –normalizeUsingRPKM –binsize 10.

Luciferase assay—The pGL3-control vector (Promega) lacking the SV40 enhancer (pGL3-noSV40) was a kind gift of the Wysocka laboratory (Prescott et al., 2015). Intact enhancers E1-E5 and E3 segments E3A-C were amplified from genomic DNA extracted from SKmel147 cells (Table S7). Mutated E3A sequence was amplified from a custom made oligo (Genscript, Table S7). Sequences were then cloned into NheI/XhoI-digested pGL3-noSV40 using In-Fusion HD Cloning Kit (Clontech). Reporter vectors were co-transfected with FuGENE 6 (Promega) at a 1:200 ratio with pRL-SV40 renilla luciferase in SKmel147 cells. Luminescence was measured using the Dual-Luciferase Reporter Assay System at 24 hr post-transfection. Luminescence measurements were performed in triplicate using SpectraMax M5 (Molecular Devices), on at least three biological replicates.

Growth Curves—For TEAD4 and FOSL2 knockdown growth curves in SKmel147 cells, lentiviral vectors were produced in HEK293T cells transfected with standard calcium phosphate method using packaging psPAX2 (Addgene #12260), pMD2.G (Addgene #12259) and plkO.1-human-shRNA (Sigma) (in a ratio 3:1:4). 48 and 72 hr post transfection supernatants were collected, consolidated (12 mL total) and filtered with a 0.45 μm filter. SKmel147 cells were infected with 500-1000 μL supernatant for 12 hr, in the presence of 8 μg/mL poly-brene (Vardabasso et al., 2015), seeded at 15,000 cells per well in a 6-well plate in triplicates, and followed for confluency using In-cuCyte (Essen BioScience). For AMIGO2 knockdown in NHM, cells were infected as above, seeded at 150,000 per well and followed using IncuCyte.

CRISPR-Cas9 genome editing—SKmel147 cells stably expressing Cas9 were generated by infection with the lentiCas9-Blast plasmid (Addgene, Cat# 52962). The sgRNAs (Table S7) were cloned using BbsI site downstream of the human U6 promoter in a lentiviral vector containing either EGFP or mCherry downstream of the human PGK promoter (kind gift of Brown laboratory, ISMMS). Lentiviral vectors were produced as above. SKmel147 cells were first infected with the lentiCas9-Blast plasmid lentiviral supernatant, and then selected with blasticydin (10 μg/mL for 10 days) for cells expressing the Cas9 nuclease. Cells were then infected with pLenti-GFP/mCherry-sgRNAs, and GFP- and/or mCherry-positive cells were sorted 2 days after infection. For clone isolation, positive single cells were sorted into 96 well plates. Clones were grown and expanded for approximately 4 weeks prior to DNA extraction for PCR-based screening (Table S7), and TOPO cloning (Invitrogen, TOPO TA Cloning Kit for Sequencing, Cat# 45-0030). For competition assays, GFP- and/or mCherry-positive cells were counted and mixed at equal numbers of SKmel147 cells expressing Cas9, and examined by FACS at day 0 and day 7.

Enhancer calling and enhancer-gene associations—Enhancers (TEs) and super-enhancers (SEs) were called based on BRD4 and H3K27ac enrichment separately in SKmel147 using the ROSE algorithm (Rank Ordering of Super-Enhancers) (Lovén et al., 2013; Whyte et al., 2013) (stitching distance 12.5kb and TSS exclusion zone size 2.5kb. BRD4/H3K27ac levels were normalized to Input control; ChIP-Input). Only BRD4/H3K27ac enhancers overlapping with significant ATAC peaks were considered. The ROSE algorithm was also used to extract H3K27ac levels within the *AMIGO2* SE in NHM1, NHM2, SKmel147, 501MEL, SKmel239 and SKmel2 (Figure 6D). ChIP-seq occupancy levels for heatmaps and meta-profiles plots were calculated using deepTools. Enhancers were associated to the closest expressed genes (nFPKM ≥ 1.5) using the BEDTools suite (Quinlan and Hall, 2010). All *MIR*, *SNORD*, *RNVU*, *SNOR*, and *RNU* genes were excluded. TEs within SEs (Figure 5F, 5G, 5I, S6A) were called based on ATAC-seq significant peaks using the BEDtools suite.

TF motif analysis—Enriched TFs DNA binding motifs *(De Novo*) were identified with a 1000bp window centered on 569 BRD4 significant peaks within the SKmel147 top 150 BRD4 SEs (Figure 5A, 5B), using HOMER suite (findMotifsGenome.pl; version 4.8) (Heinz et al., 2010). Motifs were considered based on p value ($p < 10^{-12}$) and expression levels in SKmel147.

Dendrograms—Normalized total ChIP-seq H3K27ac reads within 464 SKmel147 SEs for NHM1, NHM2, 501MEL and SKmel239 ($BRAF^{V600E}$), and SKmel2 and SKmel147 ($NRAS^{Q61R}$) melanoma cell lines were calculated using the ROSE algorithm. Correlations were calculated based on distance correlation (R; energy package). Distances were defined as 1-abs(corr) and were calculated in R, and dendrograms were drawn using a neighbor-joining algorithm (R; ape package). Normalized expression levels of 387 SE associated genes in SKmel147 across all cell lines, were used to generate the expression Dendrogram (Figure S6A).

Mosaic plots—Mosaic plots were generated using GEDI (Gene Expression Dynamics Inspector) (Eichler et al., 2003) on H3K27ac ChIP-seq signal within 5142 BRD4 identified SKmel147 TEs and SEs. H3K27ac signal across four melanoma and 2 NHM samples was calculated using ROSE. Maps of size 50×50.

GO analysis—GO terms were obtained using Enrichr (Kuleshov et al., 2016). Combined score of top categories is shown for all plots.

QUANTIFICATION AND STATISTICAL ANALYSIS

Statistical methodologies—Statistical analysis was performed using unpaired Student's t test unless otherwise indicated (for Figures 1B and 1C, paired Student's t test was used). Statistical tests performed as part of the RNA-seq, ChIP-seq, and ATAC-seq analyses are detailed in relevant sections above. Error bars for boxplots represent 10-90 percentile with outliers omitted, unless otherwise indicated. For growth curves (Figure S6H), nonlinear regression (curve fit) was used to determine significance. For competition assay (Figure

S7D), Welch's t test was used. P values are represented as *p < 0.05, **p < 0.01 and ***p < 0.001.

DATA AND SOFTWARE AVAILABILITY

Data deposition—The raw and processed sequencing data have been deposited to GEO under accession number: GSE94488. Raw data for immunoblots and for AMIGO2 Mass Spectrometry have been deposited to Mendeley Data and are available at https://doi.org/10.17632/8g4vcy4ymm.1.

Supplementary Material

Refer to Web version on PubMed Central for supplementary material.

Acknowledgments

The authors thank Jay Bradner, Jian Jin, Iman Osman, Joanna Wysocka, Tomek Swigut, and Rana Moubarak for advice and reagents; Histopathology Core, Genomics Technology Center, and Proteomics Laboratory at NYU Langone Medical Center, supported by the Cancer Center Support Grant P30CA016087 at the Laura and Isaac Perlmutter Cancer Center; and Genomics Core Facility and Gayatri Panda at Icahn School of Medicine at Mount Sinai (ISMMS) and Alicia Alonso (Epigenomics Core at Weill Cornell Medicine) for sequencing assistance. The authors also thank the Functional Proteomics RPPA Core facility, supported by MD Anderson Cancer Center Support Grant P30CA016672. This work was supported by Scientific Computing at ISMMS, Office of Research Infrastructure of the NIH to ISMMS (S10OD018522), ISMMS Cancer Center Support Grant P30CA196521, Leukemia and Lymphoma Society, Pershing Square Sohn Cancer Research Alliance, the Starr Cancer Consortium, and NIH/NCI R01CA174793 (J.-S.R. and C.R.V.); Dermatology Foundation (D.H.); Human Frontier Science Program postdoctoral fellowship and New York Stem Cell Foundation Druckenmiller postdoctoral fellowship (R.D.M.); R01CA155234 and R01CA163891 (E.H.); and Hirschl/Weill-Caulier Research Award, Melanoma Research Alliance, Harry J. Lloyd Charitable Trust, and NIH/NCI R01CA154683 (E.B.).

References

Adam RC, Yang H, Rockowitz S, Larsen SB, Nikolova M, Oristian DS, Polak L, Kadaja M, Asare A, Zheng D, Fuchs E. Pioneer factors govern super-enhancer dynamics in stem cell plasticity and lineage choice. Nature. 2015; 521:366–370. [PubMed: 25799994]

Agrawal P, Fontanals-Cirera B, Sokolova E, Jacob S, Vaiana CA, Argibay D, Davalos V, McDermott M, Nayak S, Darvishian F, et al. A Systems Biology Approach Identifies FUT8 as a Driver of Melanoma Metastasis. Cancer Cell. 2017; 31:804–819e807. [PubMed: 28609658]

Akhtar-Zaidi B, Cowper-Sal-lari R, Corradin O, Saiakhova A, Bartels CF, Balasubramanian D, Myeroff L, Lutterbaugh J, Jarrar A, Kalady MF, et al. Epigenomic enhancer profiling defines a signature of colon cancer. Science. 2012; 336:736–739. [PubMed: 22499810]

Anders L, Guenther MG, Qi J, Fan ZP, Marineau JJ, Rahl PB, Lovén J, Sigova AA, Smith WB, Lee TI, et al. Genome-wide localization of small molecules. Nat Biotechnol. 2014; 32:92–96. [PubMed: 24336317]

Bhat UG, Zipfel PA, Tyler DS, Gartel AL. Novel anticancer compounds induce apoptosis in melanoma cells. Cell Cycle. 2008; 7:1851–1855. [PubMed: 18583930]

Buenrostro JD, Giresi PG, Zaba LC, Chang HY, Greenleaf WJ. Transposition of native chromatin for fast and sensitive epigenomic profiling of open chromatin, DNA-binding proteins and nucleosome position. *Nat.* Methods. 2013; 10:1213–1218.

Buenrostro JD, Wu B, Chang HY, Greenleaf WJ. ATAC-seq: A Method for Assaying Chromatin Accessibility Genome-Wide. Curr Protoc Mol Biol. 2015; 109:21–29.

Cancer Genome Atlas, N.; Cancer Genome Atlas Network. Genomic Classification of Cutaneous Melanoma. Cell. 2015; 161:1681–1696. [PubMed: 26091043]

Ceol CJ, Houvras Y, Jane-Valbuena J, Bilodeau S, Orlando DA, Battisti V, Fritsch L, Lin WM, Hollmann TJ, Ferré F, et al. The histone methyltransferase SETDB1 is recurrently amplified in melanoma and accelerates its onset. Nature. 2011; 471:513–517. [PubMed: 21430779]

Chapman PB, Hauschild A, Robert C, Haanen JB, Ascierto P, Larkin J, Dummer R, Garbe C, Testori A, Maio M, et al. BRIM-3 Study Group. Improved survival with vemurafenib in melanoma with BRAF V600E mutation. N Engl J Med. 2011; 364:2507–2516. [PubMed: 21639808]

Chen R, Khatri P, Mazur PK, Polin M, Zheng Y, Vaka D, Hoang CD, Shrager J, Xu Y, Vicent S, et al. A meta-analysis of lung cancer gene expression identifies PTK7 as a survival gene in lung adenocarcinoma. Cancer Res. 2014; 74:2892–2902. [PubMed: 24654231]

Creyghton MP, Cheng AW, Welstead GG, Kooistra T, Carey BW, Steine EJ, Hanna J, Lodato MA, Frampton GM, Sharp PA, et al. Histone H3K27ac separates active from poised enhancers and predicts developmental state. *Proc. Natl. Acad. Sci.* USA. 2010; 107:21931–21936.

Damelin M, Bankovich A, Bernstein J, Lucas J, Chen L, Williams S, Park A, Aguilar J, Ernstoff E, Charati M, et al. A PTK7-targeted antibody-drug conjugate reduces tumor-initiating cells and induces sustained tumor regressions. Sci Transl Med. 2017; 9:eaag2611. [PubMed: 28077676]

Dawson MA, Prinjha RK, Dittmann A, Giotopoulos G, Bantscheff M, Chan WI, Robson SC, Chung CW, Hopf C, Savitski MM, et al. Inhibition of BET recruitment to chromatin as an effective treatment for MLL-fusion leukaemia. Nature. 2011; 478:529–533. [PubMed: 21964340]

de Miera EV, Friedman EB, Greenwald HS, Perle MA, Osman I. Development of five new melanoma low passage cell lines representing the clinical and genetic profile of their tumors of origin. Pigment Cell Melanoma Res. 2012; 25:395–397. [PubMed: 22404973]

Dekker J, Heard E. Structural and functional diversity of Topologically Associating Domains. FEBS Lett. 2015; 589(20 Pt A):2877–2884. [PubMed: 26348399]

Di Micco R, Fontanals-Cirera B, Low V, Ntziachristos P, Yuen SK, Lovell CD, Dolgalev I, Yonekubo Y, Zhang G, Rusinova E, et al. Control of embryonic stem cell identity by BRD4-dependent transcriptional elongation of super-enhancer-associated pluripotency genes. Cell Rep. 2014; 9:234–247. [PubMed: 25263550]

Draker R, Ng MK, Sarcinella E, Ignatchenko V, Kislinger T, Cheung P. A combination of H2A.Z and H4 acetylation recruits Brd2 to chromatin during transcriptional activation. PLoS Genet. 2012; 8:e1003047. [PubMed: 23144632]

Eichler GS, Huang S, Ingber DE. Gene Expression Dynamics Inspector (GEDI): for integrative analysis of expression profiles. Bioinformatics. 2003; 19:2321–2322. [PubMed: 14630665]

Fecher LA, Agarwala SS, Hodi FS, Weber JS. Ipilimumab and its toxicities: a multidisciplinary approach. Oncologist. 2013; 18:733–743. [PubMed: 23774827]

Filippakopoulos P, Knapp S. Targeting bromodomains: epigenetic readers of lysine acetylation. Nat Rev Drug Discov. 2014; 13:337–356. [PubMed: 24751816]

Filippakopoulos P, Qi J, Picaud S, Shen Y, Smith WB, Fedorov O, Morse EM, Keates T, Hickman TT, Felletar I, et al. Selective inhibition of BET bromodomains. Nature. 2010; 468:1067–1073. [PubMed: 20871596]

Fu Y, Lv P, Yan G, Fan H, Cheng L, Zhang F, Dang Y, Wu H, Wen B. MacroH2A1 associates with nuclear lamina and maintains chromatin architecture in mouse liver cells. Sci Rep. 2015; 5:17186. [PubMed: 26603343]

Gallagher SJ, Mijatov B, Gunatilake D, Tiffen JC, Gowrishankar K, Jin L, Pupo GM, Cullinane C, Prinjha RK, Smithers N, et al. The epigenetic regulator I-BET151 induces BIM-dependent apoptosis and cell cycle arrest of human melanoma cells. J Invest Dermatol. 2014; 134:2795–2805. [PubMed: 24906137]

Golubkov VS, Aleshin AE, Strongin AY. Potential relation of aberrant proteolysis of human protein tyrosine kinase 7 (PTK7) chuzhoi by membrane type 1 matrix metalloproteinase (MT1-MMP) to congenital defects. J Biol Chem. 2011; 286:20970–20976. [PubMed: 21518755]

Golubkov VS, Prigozhina NL, Zhang Y, Stoletov K, Lewis JD, Schwartz PE, Hoffman RM, Strongin AY. Protein-tyrosine pseudokinase 7 (PTK7) directs cancer cell motility and metastasis. J Biol Chem. 2014; 289:24238–24249. [PubMed: 25006253]

Hanssen LLP, Kassouf MT, Oudelaar AM, Biggs D, Preece C, Downes DJ, Gosden M, Sharpe JA, Sloane-Stanley JA, Hughes JR, et al. Tissue-specific CTCF-cohesin-mediated chromatin

architecture delimits enhancer interactions and function in vivo. Nat Cell Biol. 2017; 19:952–961. [PubMed: 28737770]

Hasson D, Panchenko T, Salimian KJ, Salman MU, Sekulic N, Alonso A, Warburton PE, Black BE. The octamer is the major form of CENP-A nucleosomes at human centromeres. Nat Struct Mol Biol. 2013; 20:687–695. [PubMed: 23644596]

Heinz S, Benner C, Spann N, Bertolino E, Lin YC, Laslo P, Cheng JX, Murre C, Singh H, Glass CK. Simple combinations of lineage-determining transcription factors prime cis-regulatory elements required for macrophage and B cell identities. *Mol.* Cell. 2010; 38:576–589.

Heinz S, Romanoski CE, Benner C, Glass CK. The selection and function of cell type-specific enhancers. Nat Rev Mol Cell Biol. 2015; 16:144–154. [PubMed: 25650801]

Hodis E, Watson IR, Kryukov GV, Arold ST, Imielinski M, Theurillat JP, Nickerson E, Auclair D, Li L, Place C, et al. A landscape of driver mutations in melanoma. Cell. 2012; 150:251–263. [PubMed: 22817889]

Hsu SC, Gilgenast TG, Bartman CR, Edwards CR, Stonestrom AJ, Huang P, Emerson DJ, Evans P, Werner MT, Keller CA, et al. The BET Protein BRD2 Cooperates with CTCF to Enforce Transcriptional and Architectural Boundaries. *Mol.* Cell. 2017; 66:102–116e107.

Ito T, Kohashi K, Yamada Y, Maekawa A, Kuda M, Furue M, Oda Y. Prognostic significance of forkhead box M1 (FoxM1) expression and antitumour effect of FoxM1 inhibition in melanoma. Histopathology. 2016; 69:63–71. [PubMed: 26619071]

Kanda Y, Osaki M, Onuma K, Sonoda A, Kobayashi M, Hamada J, Nicolson GL, Ochiya T, Okada F. Amigo2-upregulation in Tumour Cells Facilitates Their Attachment to Liver Endothelial Cells Resulting in Liver Metastases. Sci Rep. 2017; 7:43567. [PubMed: 28272394]

Kapoor A, Goldberg MS, Cumberland LK, Ratnakumar K, Segura MF, Emanuel PO, Menendez S, Vardabasso C, Leroy G, Vidal CI, et al. The histone variant macroH2A suppresses melanoma progression through regulation of CDK8. Nature. 2010; 468:1105–1109. [PubMed: 21179167]

Kaufman CK, Mosimann C, Fan ZP, Yang S, Thomas AJ, Ablain J, Tan JL, Fogley RD, van Rooijen E, Hagedorn EJ, et al. A zebra-fish melanoma model reveals emergence of neural crest identity during melanoma initiation. Science. 2016; 351:aad2197. [PubMed: 26823433]

Kim KB, Kefford R, Pavlick AC, Infante JR, Ribas A, Sosman JA, Fecher LA, Millward M, McArthur GA, Hwu P, et al. Phase II study of the MEK1/MEK2 inhibitor Trametinib in patients with metastatic BRAF-mutant cutaneous melanoma previously treated with or without a BRAF inhibitor. J Clin Oncol. 2013; 31:482–489. [PubMed: 23248257]

Kuja-Panula J, Kiiltomäki M, Yamashiro T, Rouhiainen A, Rauvala H. AMIGO, a transmembrane protein implicated in axon tract development, defines a novel protein family with leucine-rich repeats. J Cell Biol. 2003; 160:963–973. [PubMed: 12629050]

Kuleshov MV, Jones MR, Rouillard AD, Fernandez NF, Duan Q, Wang Z, Koplev S, Jenkins SL, Jagodnik KM, Lachmann A, et al. Enrichr: a comprehensive gene set enrichment analysis web server 2016 update. Nucleic Acids Res. 2016; 44:W90–7. [PubMed: 27141961]

Kuphal S, Wallner S, Bosserhoff AK. Impact of LIF (leukemia inhibitory factor) expression in malignant melanoma. Exp Mol Pathol. 2013; 95:156–165. [PubMed: 23831429]

Kuželová K, Grebeňova D, Brodská B. Dose-dependent effects of the caspase inhibitor Q-VD-OPh on different apoptosis-related processes. J Cell Biochem. 2011; 112:3334–3342. [PubMed: 21751237]

Langmead B, Trapnell C, Pop M, Salzberg SL. Ultrafast and memory-efficient alignment of short DNA sequences to the human genome. Genome Biol. 2009; 10:R25. [PubMed: 19261174]

Lian CG, Xu Y, Ceol C, Wu F, Larson A, Dresser K, Xu W, Tan L, Hu Y, Zhan Q, et al. Loss of 5-hydroxymethylcytosine is an epigenetic hallmark of melanoma. Cell. 2012; 150:1135–1146. [PubMed: 22980977]

Lito P, Rosen N, Solit DB. Tumor adaptation and resistance to RAF inhibitors. Nat Med. 2013; 19:1401–1409. [PubMed: 24202393]

Lovén J, Hoke HA, Lin CY, Lau A, Orlando DA, Vakoc CR, Bradner JE, Lee TI, Young RA. Selective inhibition of tumor oncogenes by disruption of super-enhancers. Cell. 2013; 153:320–334. [PubMed: 23582323]

Lu X, Borchers AG, Jolicoeur C, Rayburn H, Baker JC, Tessier-Lavigne M. PTK7/CCK-4 is a novel regulator of planar cell polarity in vertebrates. Nature. 2004; 430:93–98. [PubMed: 15229603]

Mellacheruvu D, Wright Z, Couzens AL, Lambert JP, St-Denis NA, Li T, Miteva YV, Hauri S, Sardiu ME, Low TY, et al. The CRAPome: a contaminant repository for affinity purification-mass spectrometry data. *Nat.* Methods. 2013; 10:730–736.

Mertz JA, Conery AR, Bryant BM, Sandy P, Balasubramanian S, Mele DA, Bergeron L, Sims RJ 3rd. Targeting MYC dependence in cancer by inhibiting BET bromodomains. Proc Natl Acad Sci USA. 2011; 108:16669–16674. [PubMed: 21949397]

Mirguet O, Gosmini R, Toum J, Clément CA, Barnathan M, Brusq JM, Mordaunt JE, Grimes RM, Crowe M, Pineau O, et al. Discovery of epigenetic regulator I-BET762: lead optimization to afford a clinical candidate inhibitor of the BET bromodomains. J Med Chem. 2013; 56:7501–7515. [PubMed: 24015967]

Miyashita A, Fukushima S, Nakahara S, Yamashita J, Tokuzumi A, Aoi J, Ichihara A, Kanemaru H, Jinnin M, Ihn H. Investigation of FOXM1 as a Potential New Target for Melanoma. PLoS ONE. 2015; 10:e0144241. [PubMed: 26640950]

Na HW, Shin WS, Ludwig A, Lee ST. The cytosolic domain of protein-tyrosine kinase 7 (PTK7), generated from sequential cleavage by a disintegrin and metalloprotease 17 (ADAM17) and γ-secretase, enhances cell proliferation and migration in colon cancer cells. J Biol Chem. 2012; 287:25001–25009. [PubMed: 22665490]

Ono T, Sekino-Suzuki N, Kikkawa Y, Yonekawa H, Kawashima S. Alivin 1, a novel neuronal activity-dependent gene, inhibits apoptosis and promotes survival of cerebellar granule neurons. J Neurosci. 2003; 23:5887–5896. [PubMed: 12843293]

Ooi WF, Xing M, Xu C, Yao X, Ramlee MK, Lim MC, Cao F, Lim K, Babu D, Poon LF, et al. Epigenomic profiling of primary gastric adenocarcinoma reveals super-enhancer heterogeneity. Nat Commun. 2016; 7:12983. [PubMed: 27677335]

Ozanne BW, Spence HJ, McGarry LC, Hennigan RF. Transcription factors control invasion: AP-1 the first among equals. Oncogene. 2007; 26:1–10. [PubMed: 16799638]

Park ES, Rabinovsky R, Carey M, Hennessy BT, Agarwal R, Liu W, Ju Z, Deng W, Lu Y, Woo HG, et al. Integrative analysis of proteomic signatures, mutations, and drug responsiveness in the NCI 60 cancer cell line set. Mol Cancer Ther. 2010; 9:257–267. [PubMed: 20124458]

Park H, Lee S, Shrestha P, Kim J, Park JA, Ko Y, Ban YH, Park DY, Ha SJ, Koh GY, et al. AMIGO2, a novel membrane anchor of PDK1 controls cell survival and angiogenesis via Akt activation. J Cell Biol. 2015; 211:619–637. [PubMed: 26553931]

Penna E, Orso F, Cimino D, Vercellino I, Grassi E, Quaglino E, Turco E, Taverna D. miR-214 coordinates melanoma progression by upregulating ALCAM through TFAP2 and miR-148b downmodulation. Cancer Res. 2013; 73:4098–4111. [PubMed: 23667173]

Postow MA, Chesney J, Pavlick AC, Robert C, Grossmann K, McDermott D, Linette GP, Meyer N, Giguere JK, Agarwala SS, et al. Nivolumab and ipilimumab versus ipilimumab in untreated melanoma. N Engl J Med. 2015; 372:2006–2017. [PubMed: 25891304]

Prescott SL, Srinivasan R, Marchetto MC, Grishina I, Narvaiza I, Selleri L, Gage FH, Swigut T, Wysocka J. Enhancer divergence and cis-regulatory evolution in the human and chimp neural crest. Cell. 2015; 163:68–83. [PubMed: 26365491]

Prud'homme GJ, Glinka Y. Neuropilins are multifunctional coreceptors involved in tumor initiation, growth, metastasis and immunity. Oncotarget. 2012; 3:921–939. [PubMed: 22948112]

Puissant A, Frumm SM, Alexe G, Bassil CF, Qi J, Chanthery YH, Nekritz EA, Zeid R, Gustafson WC, Greninger P, et al. Targeting MYCN in neuroblastoma by BET bromodomain inhibition. Cancer Discov. 2013; 3:308–323. [PubMed: 23430699]

Quinlan AR, Hall IM. BEDTools: a flexible suite of utilities for comparing genomic features. Bioinformatics. 2010; 26:841–842. [PubMed: 20110278]

Rabenau KE, O'Toole JM, Bassi R, Kotanides H, Witte L, Ludwig DL, Pereira DS. DEGA/AMIGO-2, a leucine-rich repeat family member, differentially expressed in human gastric adenocarcinoma: effects on ploidy, chromosomal stability, cell adhesion/migration and tumorigenicity. Oncogene. 2004; 23:5056–5067. [PubMed: 15107827]

Ramírez F, Dündar F, Diehl S, Grüning BA, Manke T. DeepTools: a flexible platform for exploring deep-sequencing data. Nucleic Acids Res. 2014; 42:W187–91. [PubMed: 24799436]

Raskin L, Fullen DR, Giordano TJ, Thomas DG, Frohm ML, Cha KB, Ahn J, Mukherjee B, Johnson TM, Gruber SB. Transcriptome profiling identifies HMGA2 as a biomarker of melanoma progression and prognosis. J Invest Dermatol. 2013; 133:2585–2592. [PubMed: 23633021]

Roe JS, Mercan F, Rivera K, Pappin DJ, Vakoc CR. BET Bromodomain Inhibition Suppresses the Function of Hematopoietic Transcription Factors in Acute Myeloid Leukemia. Mol Cell. 2015; 58:1028–1039. [PubMed: 25982114]

Segura MF, Fontanals-Cirera B, Gaziel-Sovran A, Guijarro MV, Hanniford D, Zhang G, González-Gomez P, Morante M, Jubierre L, Zhang W, et al. BRD4 sustains melanoma proliferation and represents a new target for epigenetic therapy. Cancer Res. 2013; 73:6264–6276. [PubMed: 23950209]

Souroullas GP, Jeck WR, Parker JS, Simon JM, Liu JY, Paulk J, Xiong J, Clark KS, Fedoriw Y, Qi J, et al. An oncogenic Ezh2 mutation induces tumors through global redistribution of histone 3 lysine 27 trimethylation. Nat Med. 2016; 22:632–640. [PubMed: 27135738]

Surface LE, Fields PA, Subramanian V, Behmer R, Udeshi N, Peach SE, Carr SA, Jaffe JD, Boyer LA. H2A.Z.1 Monoubiquitylation Antagonizes BRD2 to Maintain Poised Chromatin in ESCs. Cell Rep. 2016; 14:1142–1155. [PubMed: 26804911]

Tian B, Yang J, Brasier AR. Two-step cross-linking for analysis of protein-chromatin interactions. Methods Mol Biol. 2012; 809:105–120. [PubMed: 22113271]

Trapnell C, Roberts A, Goff L, Pertea G, Kim D, Kelley DR, Pimentel H, Salzberg SL, Rinn JL, Pachter L. Differential gene and transcript expression analysis of RNA-seq experiments with TopHat and Cufflinks. Nat Protoc. 2012; 7:562–578. [PubMed: 22383036]

Valiente M, Obenauf AC, Jin X, Chen Q, Zhang XH, Lee DJ, Chaft JE, Kris MG, Huse JT, Brogi E, Massagué J. Serpins promote cancer cell survival and vascular co-option in brain metastasis. Cell. 2014; 156:1002–1016. [PubMed: 24581498]

Vardabasso C, Gaspar-Maia A, Hasson D, Pünzeler S, Valle-Garcia D, Straub T, Keilhauer EC, Strub T, Dong J, Panda T, et al. Histone Variant H2A.Z.2 Mediates Proliferation and Drug Sensitivity of Malignant Melanoma. *Mol.* Cell. 2015; 59:75–88.

Verfaillie A, Imrichova H, Atak ZK, Dewaele M, Rambow F, Hulselmans G, Christiaens V, Svetlichnyy D, Luciani F, Van den Mooter L, et al. Decoding the regulatory landscape of melanoma reveals TEADS as regulators of the invasive cell state. Nat Commun. 2015; 6:6683. [PubMed: 25865119]

Vízkeleti L, Ecsedi S, Rákosy Z, Orosz A, Lázár V, Emri G, Koroknai V, Kiss T, Ádány R, Balázs M. The role of CCND1 alterations during the progression of cutaneous malignant melanoma. Tumour Biol. 2012; 33:2189–2199. [PubMed: 23001925]

Whiteman DC, Green AC, Olsen CM. The Growing Burden of Invasive Melanoma: Projections of Incidence Rates and Numbers of New Cases in Six Susceptible Populations through 2031. J Invest Dermatol. 2016; 136:1161–1171. [PubMed: 26902923]

Whyte WA, Orlando DA, Hnisz D, Abraham BJ, Lin CY, Kagey MH, Rahl PB, Lee TI, Young RA. Master transcription factors and mediator establish super-enhancers at key cell identity genes. Cell. 2013; 153:307–319. [PubMed: 23582322]

Xiang G, Yi Y, Weiwei H, Weiming W. TGIF1 promoted the growth and migration of cancer cells in nonsmall cell lung cancer. Tumour Biol. 2015; 36:9303–9310. [PubMed: 26104768]

Xu L, Shen SS, Hoshida Y, Subramanian A, Ross K, Brunet JP, Wagner SN, Ramaswamy S, Mesirov JP, Hynes RO. Gene expression changes in an animal melanoma model correlate with aggressiveness of human melanoma metastases. Mol Cancer Res. 2008; 6:760–769. [PubMed: 18505921]

Zhang Y, Liu T, Meyer CA, Eeckhoute J, Johnson DS, Bernstein BE, Nusbaum C, Myers RM, Brown M, Li W, Liu XS. Model-based analysis of ChIP-Seq (MACS). Genome Biol. 2008; 9:R137. [PubMed: 18798982]

Zhang P, Huang C, Fu C, Tian Y, Hu Y, Wang B, Strasner A, Song Y, Song E. Cordycepin (3′-deoxyadenosine) suppressed HMGA2, Twist1 and ZEB1-dependent melanoma invasion and metastasis by targeting miR-33b. Oncotarget. 2015; 6:9834–9853. [PubMed: 25868853]

Zingg D, Debbache J, Schaefer SM, Tuncer E, Frommel SC, Cheng P, Arenas-Ramirez N, Haeusel J, Zhang Y, Bonalli M, et al. The epigenetic modifier EZH2 controls melanoma growth and

metastasis through silencing of distinct tumour suppressors. Nat Commun. 2015; 6:6051. [PubMed: 25609585]

Highlights

- BET target analysis reveals pro-tumorigenic genes in melanoma cells
- The transmembrane molecule AMIGO2 and its interactor PTK7 regulate melanoma cell survival
- AMIGO2 expression is controlled by BET proteins and FOSL/TEAD TFs
- The AMIGO2-PTK7 axis represents a potential therapeutic target for melanoma

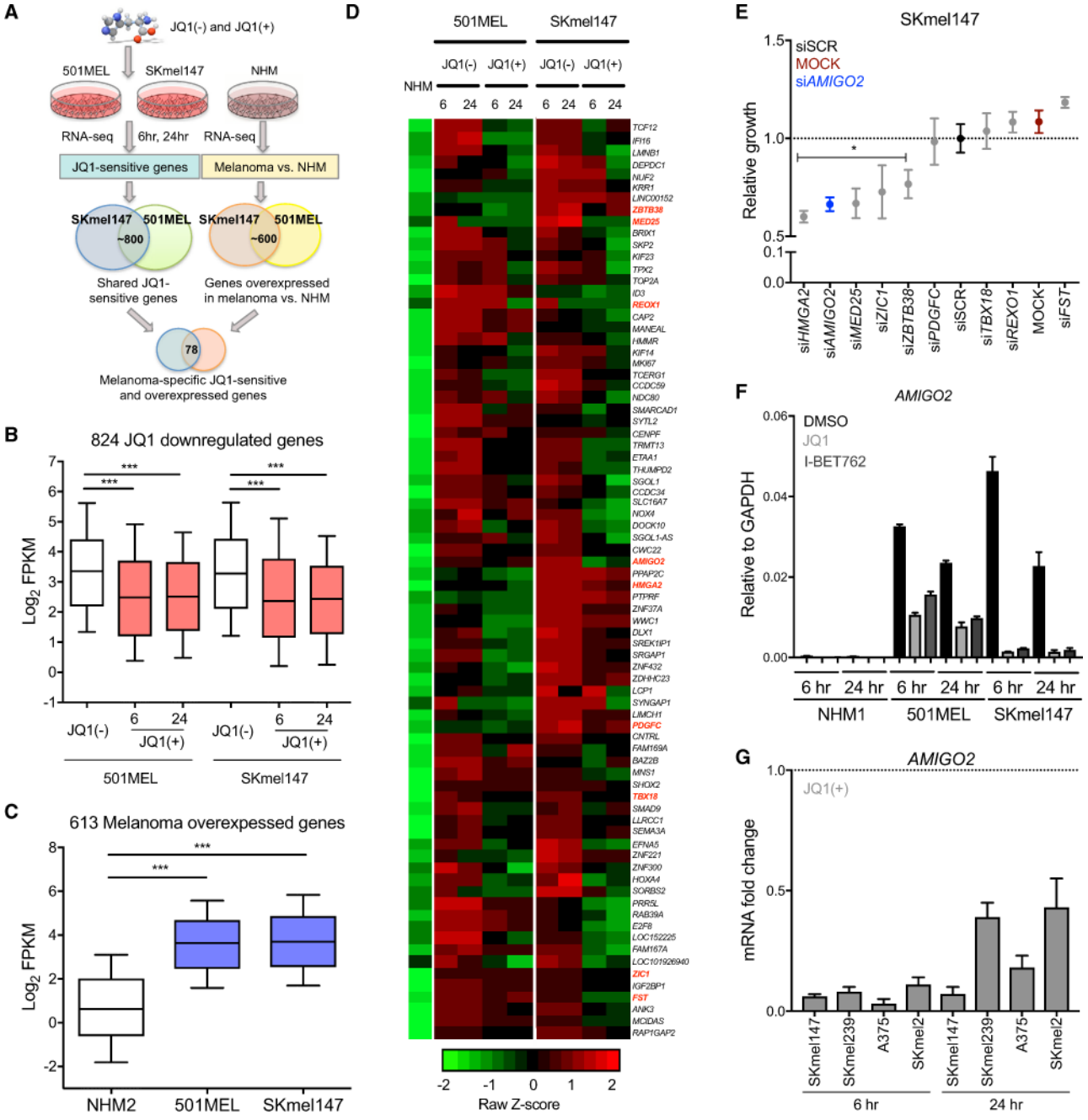

Figure 1. BETi Regulates Expression of Putative Melanoma Drivers

(A) Schematic flowchart of the integrative transcriptional profiling (RNA-seq) of metastatic melanoma cell lines and NHM.

(B) Log_2FPKM (normalized fragments per kilobase per million mapped reads) of 824 JQ1-sensitive genes, shared between both melanoma lines. Bars represent 10–90 percentile.

(C) Log_2FPKM of 613 genes overexpressed in both melanoma lines over NHM2. Bars represent 10–90 percentile.

(D) Heatmap of 78 genes that are the intersection of the 824 JQ1-sensitive (significantly downregulated) after 6 and/or 24 hr as in (B), and 613 genes overexpressed as in (C). Each row represents the transformed raw *Z* score of FPKM of an individual gene.
(E) Loss-of-function proliferation mini-screen of 9 selected genes (of 78 in D) (marked in red). Data are represented as mean ± SEM.
(F) *AMIGO2* qRT-PCR analysis of NHM1, 501MEL, and SKmel147 cells treated with DMSO, JQ1 (JQ1[+]), or I-BET762 for 6 and 24 hr. Data are represented as mean ± SEM mRNA levels normalized to *GAPDH*.
(G) *AMIGO2* qRT-PCR analysis of SKmel147, SKmel239, A375, and SKmel2 cells treated with JQ1 (JQ1[+]) for 6 and 24 hr. Data are represented as mean ± SEM and relative to DMSO. mRNA levels are normalized to *GAPDH*.
See also Figure S1 and primary data in Table S1.

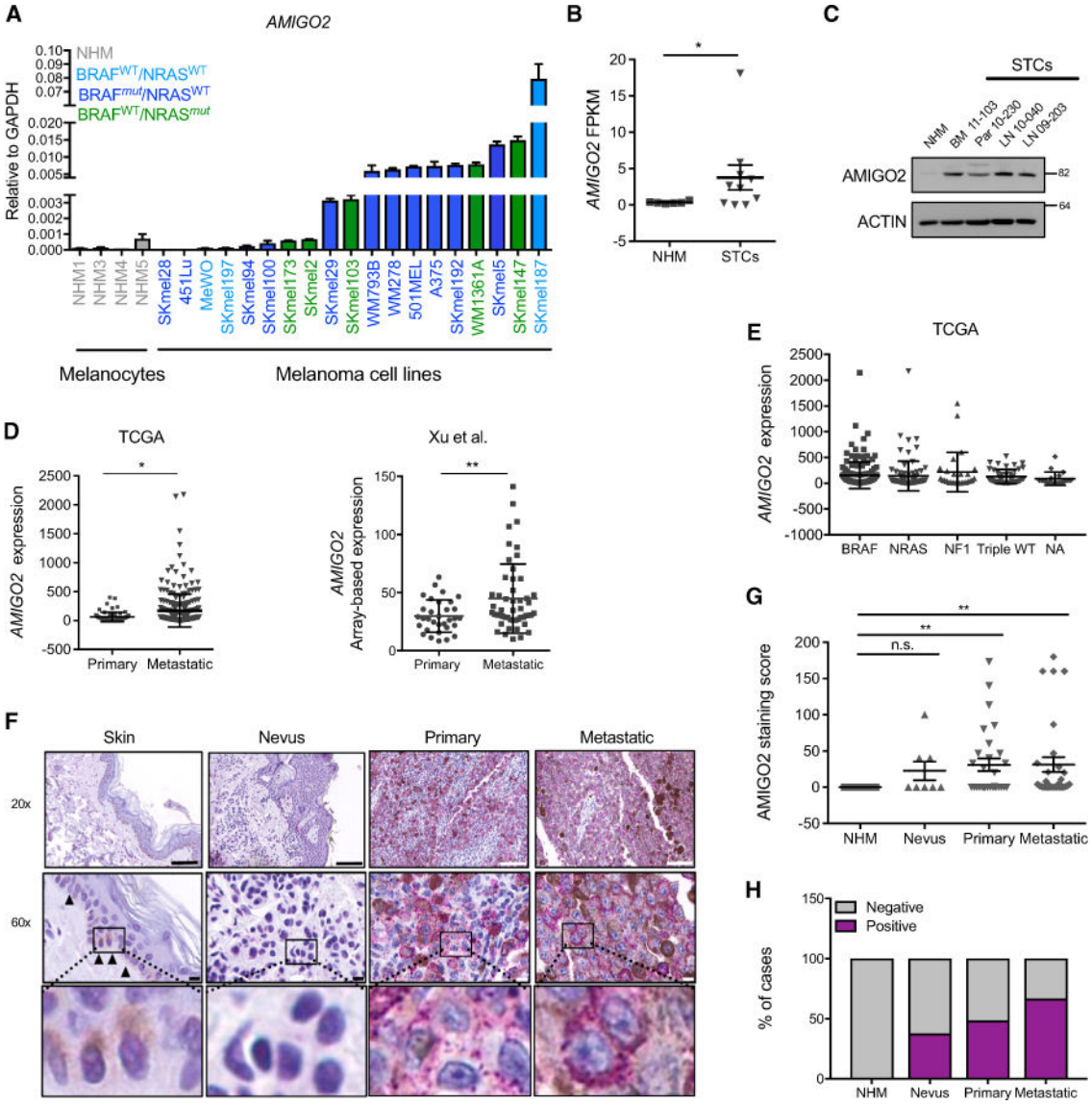

Figure 2. AMIGO2 Is Overexpressed in Human Melanoma

(A) *AMIGO2* expression levels detected by qRT-PCR in NHM and a panel of metastatic melanoma cell lines harboring distinct melanoma mutations. Data are normalized to *GAPDH*.

(B and C) *AMIGO2* mRNA detected by RNA-seq (B), and protein levels of NHM and patient-derived melanoma short-term cultures (STCs) (C). Data in (B) are represented in FPKM.

(D) *AMIGO2* mRNA levels in primary and metastatic melanoma tissue samples from TCGA (RESM-normalized values) and Xu et al., 2008 (GSE8401) (array-based expression). RNA-seq was performed by expectation-maximization.

(E) *AMIGO2* mRNA from TCGA samples grouped by mutational status. Data are represented in RESM.

(F) Immunohistochemistry (IHC) for AMIGO2 in normal skin (n = 9, NHM are marked with arrows), nevi (n = 8), primary melanoma (n = 30), and metastatic melanoma (n = 30).

Representative micrographs at 20× and 60× are shown; blow ups of representative cells are shown below. Scale bar, 100 μm.

(G) Quantified IHC scores of (F) (arbitrary units).

(H) Percent distribution of AMIGO2 cases by tissue type.

All error bars represent mean ± SD. See also primary data in Table S2.

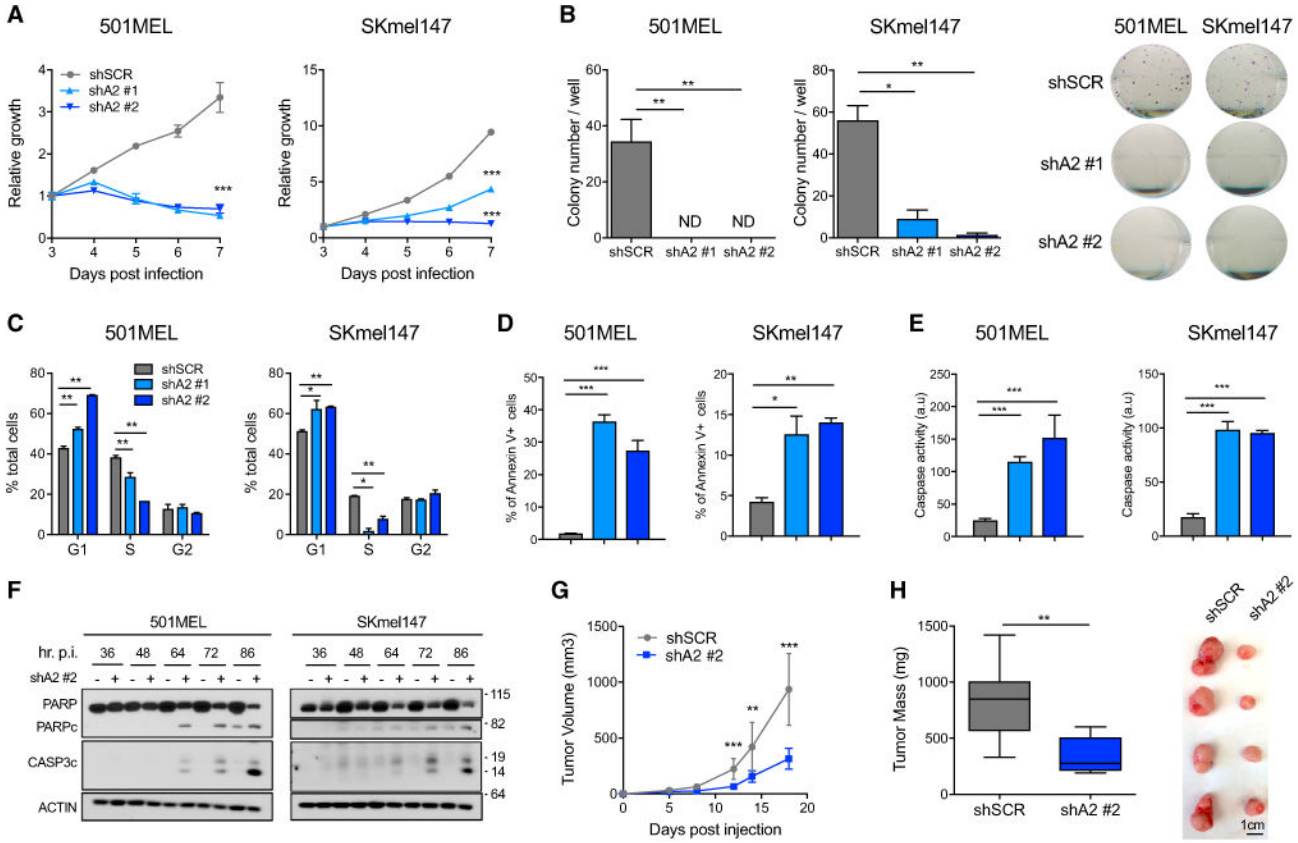

Figure 3. AMIGO2 Functions as a Pro-proliferation and Pro-survival Factor in Melanoma

(A) Relative growth curves of 501MEL and SKmel147 cells stably transduced with non-targeting scrambled control shRNA (shSCR) and two *AMIGO2* shRNAs (shA2 #1 and #2). Values are normalized to seeding control (n = 3).

(B) Colony formation assay 14 days post-infection as in (A); representative images are shown on the right.

(C) Percent of cells in G1, S, and G2 for same cells as in (A), 48 hr post-transduction.

(D) Percent of Annexin V-positive 501MEL and SKmel147 cells 5 days post-transduction.

(E) Caspase-3 activity in whole-cell extracts of same cells as in (D).

(F) PARP and cleaved CASP3 immunoblots of whole-cell lysates from 501MEL and SKmel147 cells. Actin was used as a loading control.

(G) Average tumor volume in mice injected with shSCR or shA2 #2-transduced SKmel147 cells.

(H) Average tumor mass and representative images of resected tumors taken 18 days post-injection (scale bar, 1 cm). Representative experiment is shown (n = 3).

All values and error bars represent mean ± SD or ± SEM. See also Figures S2 and S3.

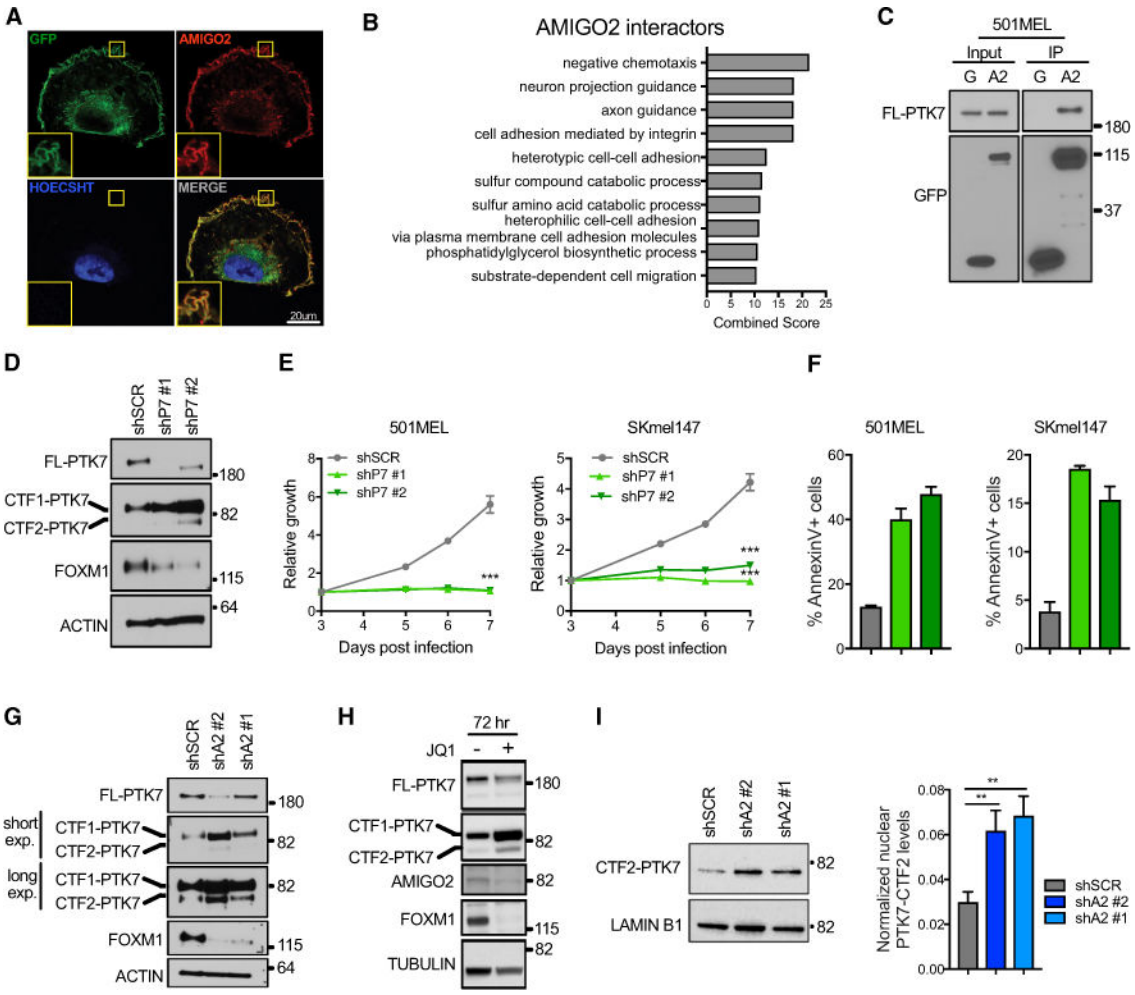

Figure 4. AMIGO2 Interacts with PTK7 and Modulates Its Processing to Promote Melanoma Survival

(A) Immunofluorescence of SKmel147 cells stably expressing AMIGO2-GFP (green), stained with AMIGO2 antibody (red) and Hoechst 33342 (blue). Scale bar, 20 μm.

(B) Functional annotation of AMIGO2-interacting proteins detected by GFP pull-down followed by MS in SKmel147 cells stably expressing AMIGO2-GFP (see Table S4).

(C) PTK7 and GFP immunoblots following GFP pull-down from 501MEL cells stably expressing AMIGO2-GFP.

(D) Full-length PTK7 (FL-PTK7), C-terminal fragments CTF1- and CTF2-PTK7, and FOXM1 immunoblots of 501MEL cells 72 hr post-infection with shSCR or sh*PTK7* (shP7 #1 and #2). Actin was used as a loading control.

(E) Relative growth curves of 501MEL (left) and SKmel147 (right) cells stably transduced with shSCR or sh*PTK7* (shP7 #1 and #2). Values are normalized to seeding control (n = 3).

(F) Percent Annexin V-positive cells 6 days post-transduction for same cells as in (E).

(G) FL-PTK7, CTF-PTK7, and FOXM1 immunoblots of 501MEL cells 48 hr post-transduction with shSCR or sh*AMIGO2* (shA2 #1 and #2). Actin was used as a loading control.

(H) FL-PTK7, CTF-PTK7, FOXM1, and AMIGO2 immunoblots of 501MEL cells untreated or treated with JQ1 (JQ1[+]) for 72 hr. Tubulin was used as a loading control.
(I) CTF2-PTK7 immunoblot of nuclear lysates from same cell as in (G) (left). Lamin B1 was used as loading control. Signal quantification (right), normalized to Lamin B1, relative to shSCR (n = 3).
All values and error bars represent mean ± SD or ± SEM. See also Figures S3 and S4.

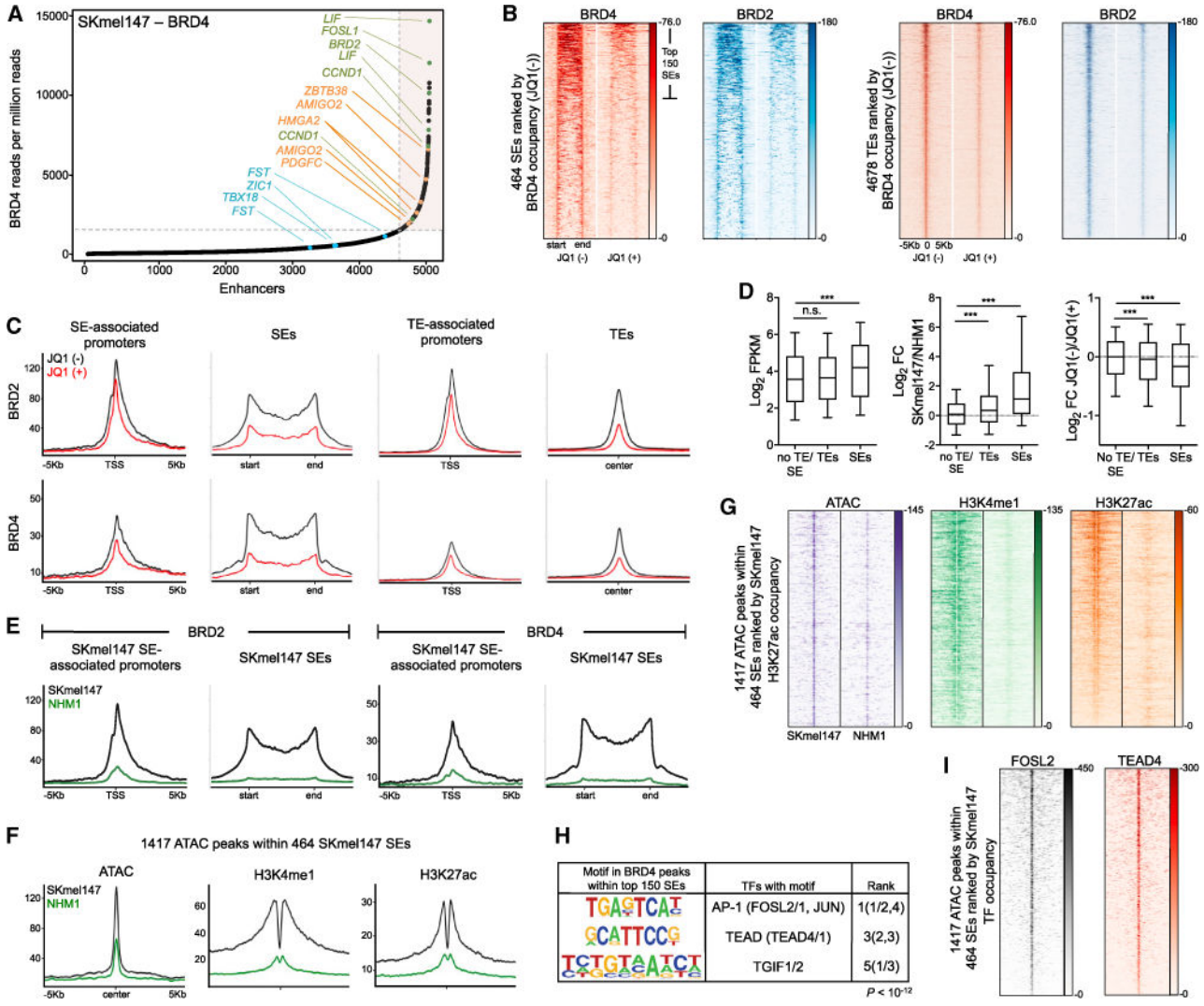

Figure 5. BRD4 and BRD2 Occupancy at Enhancers and Promoters Associates with Increased Gene Expression in Melanoma

(A) Rank order of BRD4 reads at enhancer loci in SKmel147. SEs are shown in shaded area at top right. SEs associated with known pro-tumorigenic genes (green) and SEs (orange)/TEs (blue) associated with the genes from mini-screen (Figure 1E) are shown.

(B) Heatmaps of ChIP-seq reads for BRD4 and BRD2 JQ1(−)/JQ1(+) (6 hr). Data are centered on ±1 kb window around 464 SKmel147 SEs scaled to 2 kb (left) and ±5 kb window around 4,678 TEs (right). The top 150 SEs used in (H) are indicated.

(C) BRD2 (top) and BRD4 (bottom) ChIP-seq meta-profiles in SKmel147 (JQ1[−], black; JQ1[+], red). Plots represent average read counts per 20 bp bins.

(D) Log_2FPKM of ~10,000 non-TE/non-SE-, 2,537 TE-, and 387 SE-associated genes in SKmel147 (left); log_2 fold change (log_2FC) FPKM SKmel147 over NHM1 (middle); and log_2FC FPKM SKmel147 JQ1(−)/JQ1(+) (right). Boxplots represent Tukey boxplots with outliers omitted.

(E) BRD2 (left) and BRD4 (right) ChIP-seq meta-profiles in SKmel147 (black) and NHM1 (green) at 464 SKmel147 SEs and SE-associated promoters.

(F) ATAC-seq, H3K4me1, and H3K27ac ChIP-seq meta-profiles in SKmel147 (black) and NHM1 (green).
(G) Heatmaps for ATAC-seq and ChIP-seq for H3K4me1 and H3K27ac. SKmel147 is shown at left and NHM1 at right.
(H) TF motif analysis of top 150 SEs in SKmel147.
(I) Heatmaps for ChIP-seq in SKmel147 for FOSL2 (left) and TEAD4 (right).
See also Figures S5 and S6 and primary data in Tables S1 and S5.

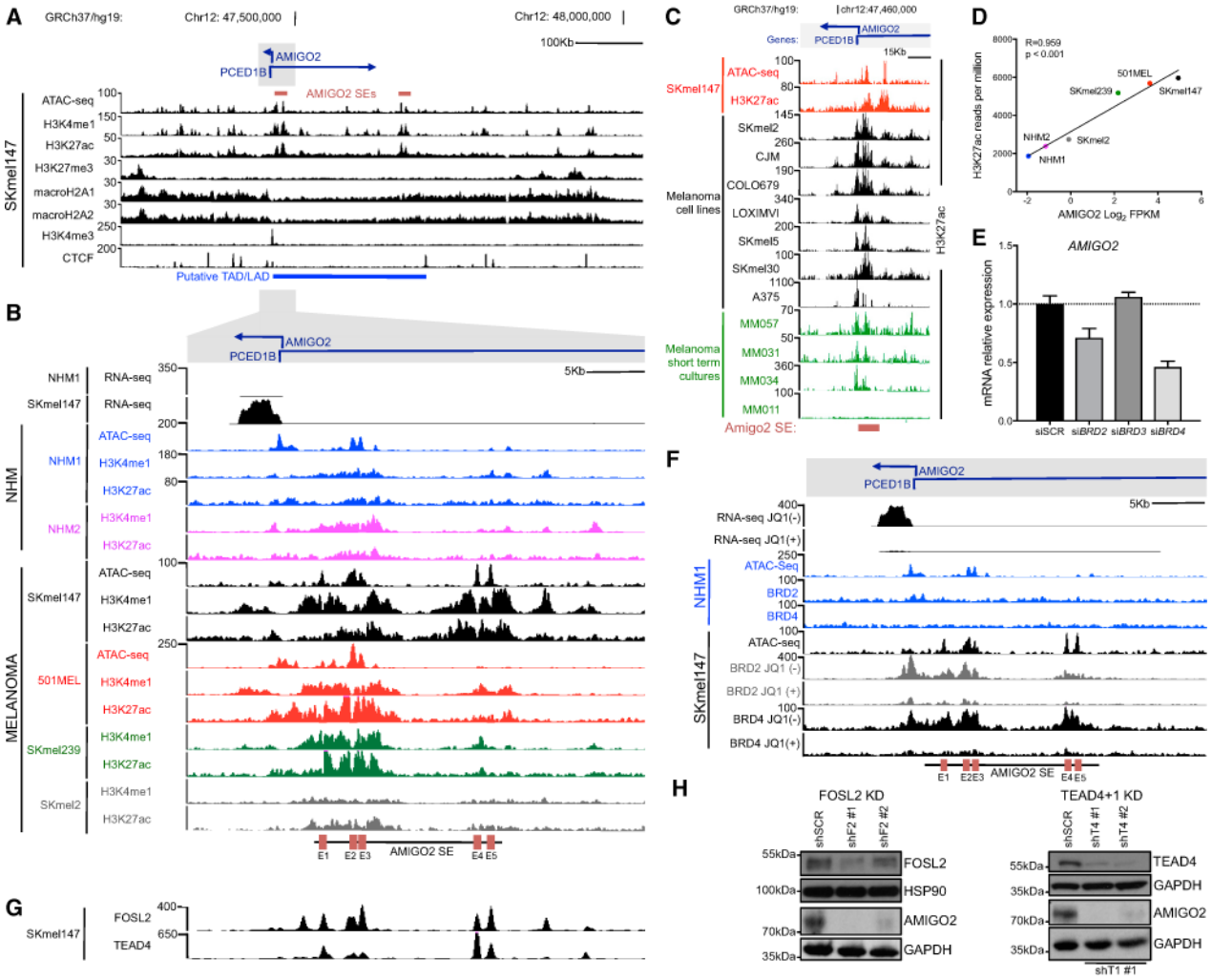

Figure 6. *AMIGO2* Expression Is Controlled by BETs and AP1/TEAD TFs

(A) Capture of the UCSC genome browser (GRCh37/hg19) showing 800 kb region on human chromosome 12 (y axis = reads per kilobase per million reads). Ensembl genes (blue) and *AMIGO2* SEs (red) are shown at the top. Putative TAD/LAD domain is shown at the bottom.

(B) Zoom-in of the *AMIGO2* locus showing 40 kb. Five TEs, E1–E5 (red), within the *AMIGO2* SE are shown (bottom).

(C) Approximately 60 kb region around the *AMIGO2* SE. ChIP-seq was performed for H3K27ac for seven additional melanoma cell lines (black) and four melanoma STCs (green) (Kaufman et al., 2016; Verfaillie et al., 2015). *AMIGO2* SE is shown at the bottom (red).

(D) Pearson correlation of number of H3K27ac reads within the *AMIGO2* SE and *AMIGO2* Log_2FPKM (Table S1).

(E) *AMIGO2* qRT-PCR in SKmel147 cells following depletion of BRD2, BRD3, or BRD4. Data are represented as mean ± SEM and normalized to *PPIA*.

(F) *AMIGO2* locus as in (B). SKmel147 RNA-seq JQ1(−)/JQ1(+) 6 hr is shown at top.

(G) *AMIGO2* locus as in (B).

(H) FOSL2 (left), TEAD4 (right), and AMIGO2 immunoblots of SKmel147 cells 96 hr post-transduction with shSCR or sh*FOSL2* (shF2 #1 and #2), and shSCR or sh*TEAD4+TEAD1* (shT4 #1+shT1 #1 and shT4 #2+shT1 #1). HSP90 and GAPDH were used as loading controls.

See also Figure S6.

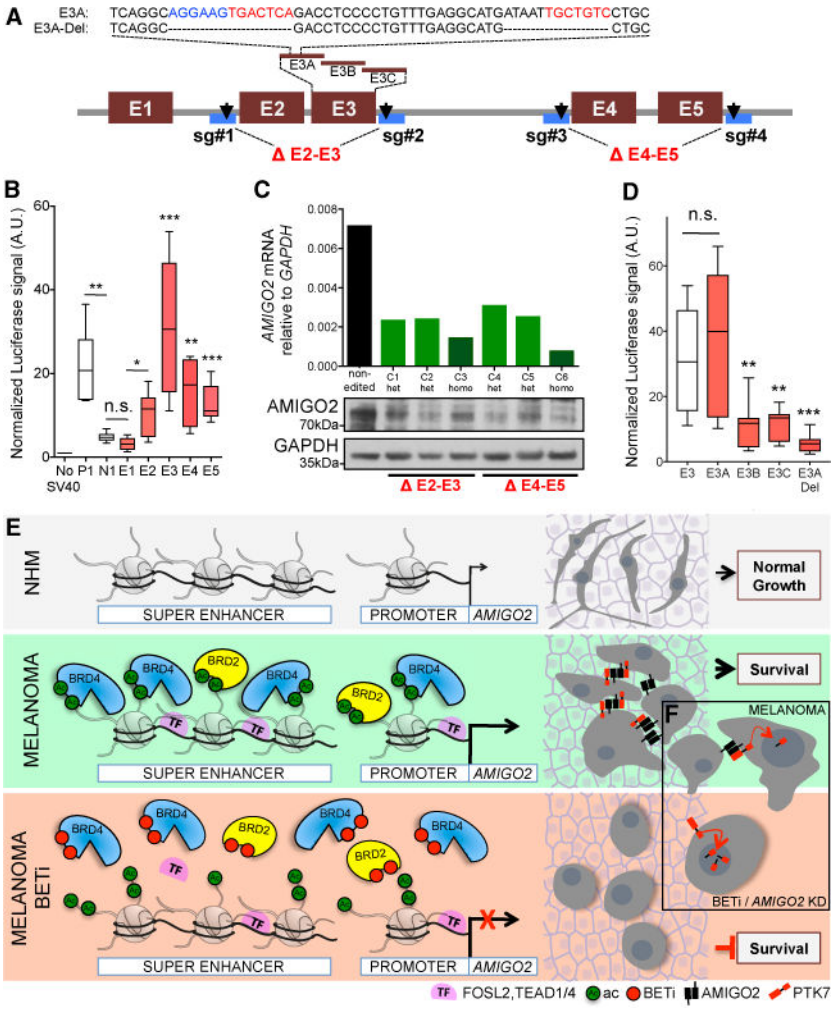

Figure 7. *AMIGO2* Expression Is Regulated by Its Proximal Upstream SE

(A) Schematic of *AMIGO2* SE showing enhancers E1–E5 (B), deleted sequences for CRISPR-Cas9 editing (C), and DNA segments used for E3 lucif-erase assay (D).

(B) Luciferase reporter assays performed in SKmel147 cells. Negative (N1) and positive (P1) controls are shown (Figure S7A). Luciferase signal was normalized to renilla transfection control. Box-plots represent Tukey boxplots with outliers omitted.

(C) CRISPR-Cas9-mediated editing of constituent enhancers E2–E3 (clones C1–C3) and E4–E5 (clones C4–C6). *AMIGO2* mRNA levels by qRT-PCR (top; data represented as mean and normalized to *GAPDH*) and AMIGO2 immunoblots of edited SKmel147 cells (bottom) with GAPDH as loading control are shown. Non-edited clone was used as negative control.

(D) Luciferase reporter assays performed in SKmel147 cells for *AMIGO2* enhancer elements E3A–C and E3A deleted for TF motifs (E3A-Del) (A). Boxplots represent Tukey boxplots with outliers omitted.

(E) Model of BET-regulated *AMIGO2* expression in melanoma and upon BETi. NHMs express low levels of *AMIGO2* due to lack of active SEs. Upon transformation, increased levels of BRD2 and BRD4 and alterations in TFs FOSL2 and TEAD4/1 trigger global epigenomic remodeling involving acquisition of SEs and activation of key melanoma

survival genes, such as *AMIGO2*. Upon BETi treatment, BET proteins are displaced from SEs and promoters, inducing gene silencing, such as the case of *AMIGO2*. Since melanoma is dependent on BETs to maintain its proliferation and survival, BETi produces cytostatic and/or cytotoxic effects on melanoma cells.

(F) AMIGO2 interacts with PTK7 and prevents nuclear accumulation of CTF2-PTK7. Upon BETi or AMIGO2 KD (knockdown), CTF2-PTK7 nuclear levels increase, possibly leading to changes in gene expression.

See also Figure S7 and primary data in Table S7.